AN ABSTRACT OF THE THESIS OF

William C Farrow III for the degree of Master of Science in Civil Engineering presented on November 19, 2002.
Title: Shear Capacity Assessment of Corrosion-Damaged Reinforced Concrete Beams

Abstract Approved:
Redacted for privacy

Christopher C. Higgins

The research presented here is a study to determine the effect of shear reinforcement corrosion on the shear capacity in conventionally reinforced concrete (CRC) bridge elements. A total of 14 CRC beams were tested using three stirrup spacings (8, 10, and 12-inch). Six of the beams included the influence of a 4-inch thick deck, and both positive and negative moment regions were considered. The CRC beams were subjected to an accelerated corrosion process to produce the damage states. Inspection techniques were used to visually correlate corrosion damage with actual structural performance. Severe corrosion damage was shown to have significant effect on the shear performance of the CRC beams. Findings indicate that current inspection ratings for corrosion damage may not adequately identify the extent of structural deterioration.

©Copyright by William C. Farrow III
November 19, 2002
All rights reserved

Shear Capacity Assessment of Corrosion-Damaged Reinforced Concrete Beams

by
William C. Farrow III

A THESIS

Submitted to

Oregon State University

In partial fulfillment of
the requirements for the
degree of

Master of Science

Presented November 19, 2002
Commencement June 2003

Master of Science thesis of William C. Farrow III presented on November 19, 2002.

APPROVED:

Redacted for privacy

Major Professor, representing Civil Engineering

Redacted for privacy

Head of the Department of Civil, Construction, and Environmental Engineering

Redacted for privacy

Dean of the Graduate School

I understand that my thesis will become part of the permanent collection of Oregon State University libraries. My signature below authorizes release of my thesis to any reader upon request.

Redacted for privacy

William C. Farrow III, Author

ACKNOWLEDGEMENTS

The author would like to thank the following people for their assistance, backing, and contribution to this research. First, I would like to thank my major professor, Dr. Christopher Higgins, for his guidance and support throughout the research. To Dr. Thomas Miller and Dr. Solomon Yim for their additional guidance. To fellow graduate students, James Newell and Tanarat Potisuk. To Lani Evans and Melissa Robello. The following personnel from the Albany Research Center for their assistance with understanding corrosion in concrete: Sophie J. Bullard, Bernard S. Covino Jr., Steve D. Cramer, Gordon R. Holcomb, and James H. Russell. Finally, to the Oregon Department of Transportation for funding and technical information, especially Steve Soltesz and Jeff Swanstrom.

TABLE OF CONTENTS

LIST OF FIGURES

LIST OF FIGURES (CONTINUED)

Figure Page

LIST OF FIGURES (CONTINUED)

Figure Page

LIST OF TABLES

Shear Capacity Assessment of Corrosion-Damaged Reinforced Concrete Beams

1.0 Introduction

A Federal Highway Administration report indicated that as of 1998 there were 235,151 conventionally reinforced concrete (CRC) bridges in service on the federal highway system with 21,164 rated as structurally deficient. A recent study (FHWA, 2002) attributed most of the structural deficiencies for CRC bridges to corrosion damage, although a comprehensive study has not been undertaken to quantify the actual number of corrosion damaged CRC bridges. The majority of deficient CRC bridges were constructed prior to the 1960's and are at the end of their intended design life. Due to the large numbers of deficient bridges and the lack of resources, there is a need to keep these aging bridges in service even as they are subject to increased volume and weight of truck traffic. Transportation officials must make decisions for postings, repair, or replacement of these bridges, based on inspections, analysis, and ratings. Currently, non-destructive test (NDT) methods are available to identify the presence of corrosion activity and to determine whether chloride thresholds have been exceeded. However, no methods currently exist to accurately correlate visual damage states and rating categories to structural performance. There is a need for more quantifiable information to correlate visual distress to the actual load carrying capacity of a structural element.

In recent years, investigators have begun to study the effects of corrosion on CRC element performance. Past research has focused in three areas: (1) flexural

behavior of members, (2) bond-slip behavior of rebar, and (3) mechanical properties of the corroded rebar. No studies of corrosion effects on shear behavior of CRC bridge elements have been performed.

This research addresses the behavior of 1950's vintage CRC bridge beams subjected to corrosion of shear reinforcement. The study focuses on accelerated corrosion-damage to large-size beam specimens, visual distress characterization, and structural tests to destruction. The results will aid in determining capacity loss of in-service beams.

2.0Background

2.1 Shear Design of CRC Beams

Shear design methodologies for CRC beams have evolved over the years. This evolution was well documented in a recent ASCE-ACI Committee 445 (1999). Design of CRC highway bridge girders currently employs two different approaches. The first is the AASHTO 16th Edition of the Standard Specification for Highway Bridges (1996), which uses the general ACI method (ACI 318, 2002). The second is the AASHTO LRFD (2001) provisions, which uses modified compression field theory (MCFT).

2.2Corrosion of CRC Elements

Past research has focused in three areas: (1) flexural behavior of members, (2) bond-slip behavior of rebar, and (3) mechanical properties of the corroded rebar. The behavior of corrosion damaged CRC elements tested in flexure indicated that as the reinforcing steel corrodes, there is a reduction in load capacity and the overall deflections increase (Al-Sulaimani et al., 1990, Almusallam et al., 1996, Cabrera, 1996). Bond-slip behavior of corroded rebar samples shows a loss of bond with increasing section loss (Al-Sulaimani et al., 1990, Cabrera, 1996, Amleh and Mirza, 1999, Stanish et al., 1999). Tensile strength of corroded rebar has been shown to be little affected, but the overall ductility can be significantly reduced (Almusallam, 2001, Palsson and Mirza,

2002). No investigation of the role of corrosion on shear behavior has been undertaken.

Corrosion of reinforcing steel in concrete occurs from two common sources: (1) chloride contamination, and (2) carbonation of the concrete. Concrete generally provides inherent corrosion protection for embedded rebar, but due to the permeability of concrete, chlorides can reach sufficient levels to cause corrosion. Once chloride concentrations are sufficiently high at the level of the reinforcement steel (15% of weight of cement (ACI, 2002)), the passive layer is disrupted and corrosion can be initiated. The most common reaction that takes place at the reinforcing steel has two parts, the anode reaction that takes the form of:

$$Fe \rightarrow Fe^{++} + 2e^{-} \qquad [1]$$

and the reaction at the cathode that is:

$$2H_2O + O_2 + 4e^{-} \rightarrow 4OH^{-} \qquad [2]$$

The corrosion reaction is completed when the Fe^{++} and the OH^{-} react with each other and form the final iron oxide rust product:

$$Fe^{++} + 2OH^{-} \rightarrow Fe(OH)_2 \qquad [3]$$

This is just one of the possible reactions that can take place during the corrosion process. Due to the non-homogenous nature of the concrete, various other reactions are possible and depend on the relative amounts of water and oxygen (Kay, 1992, Bentur et al., 1997).

There are many sources for possible chloride contamination of concrete bridges. Chlorides were sometimes introduced in the concrete at the time of construction. This occurred as a result of using beach sand, or by adding salt during cold weather to prevent freezing. Additionally, some early admixtures for accelerating curing were a source of chlorides. In coastal areas, wind-born salts can be blown on to structures, and in colder regions, salts are placed on the roadway as de-icing agents. Salts can eventually permeate through the concrete and initiate corrosion. Locations at risk for chloride contact on a typical CRC bridge section are illustrated in Figure 1. The higher risk areas for chloride contamination are the top of the deck surface, which can be under attack from de-icing salts and the interior of bridge girders and underside of the deck, from wind-born ocean salts. The fascia girder is typically at lesser risk since washing of the girder can occur from rainfall. However, the fascia girder may have increased risk in areas near bridge scuppers (drains).

Carbonation occurs when air, water, and carbon dioxide permeate into the concrete and react with calcium hydroxide, a product of concrete hydration, and form calcium carbonate. This reaction lowers the pH of the concrete making the steel more susceptible to corrosion.

The time required for chloride penetration and carbonation to occur is dependent on the permeability of the concrete. Vintage concrete mixes did not employ admixtures that are commonly available today that can reduce diffusion coefficients. A review of data available for vintage 1950's coastal

CRC bridges in Oregon indicates diffusion coefficients in the range of $9.9x10^{12}$ to $1.4x10^{-10}$ ft^2/s (Covino et al., 1999, Cramer et al., 2002). Another important factor is the amount of clear-cover concrete used to protect the steel. The 6th Edition AASHTO Standard Specification (AASHTO, 1953) specifies a minimum clear-cover of 2.0-inches. However, review of typical bridge plans from the 1950's indicates a clear-cover of 1.5-inches for shear reinforcement. Actual clear-cover for shear reinforcement can vary considerably. Based on discussions with ODOT bridge inspectors, actual clear-cover may be closer to 1-inch.

Typical distress that occurs to CRC bridge elements from corrosion is concrete cracking, rust staining, delaminations, and concrete spalling. Cracking typically occurs over the rebar and can be influenced by service loads (Francois and Arliguie, 1998). Typical concrete cracking, spalling, and reinforcement corrosion observed on 1940's-50's vintage concrete bridges is shown in Figures 2-3. Figure 2 illustrates a corrosion-damaged girder from a 1954 bridge that has been removed from service. The girder depicts the rust staining (marked with an A in the figure), fracture and/or complete section loss of stirrups (marked with a B), and areas of spalls and/or delaminations (marked with a C). Figure 3 shows an in-service bridge with multiple discontinuous stirrups from corrosion, complete spalling of the bottom cover of the concrete, and some loss of side cover.

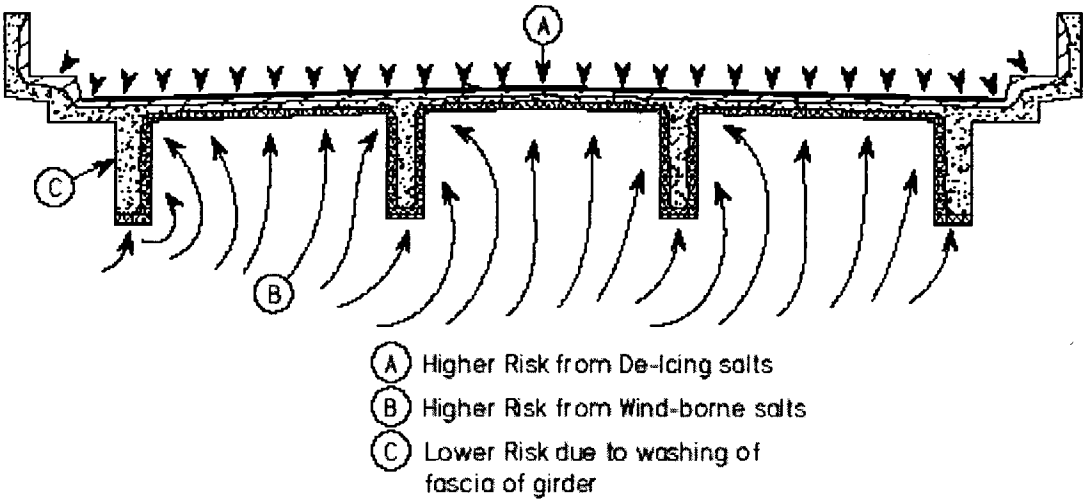

Figure 1: Mechanisms for chloride contact on RC bridge elements.

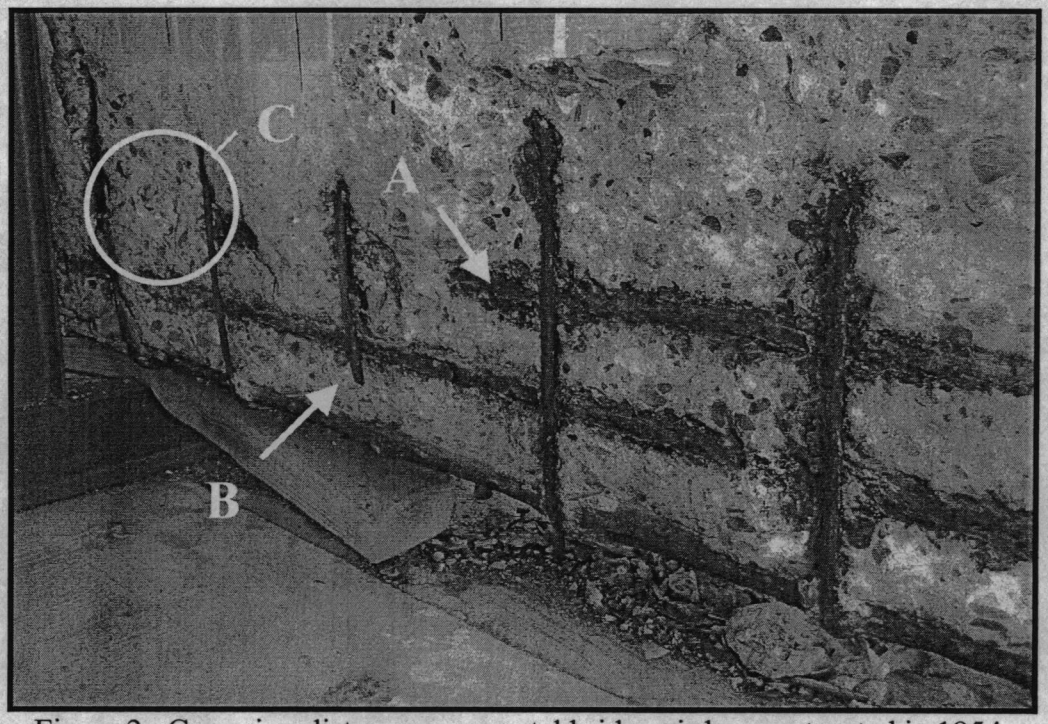

Figure 2: Corrosion distress on a coastal bridge girder constructed in 1954.

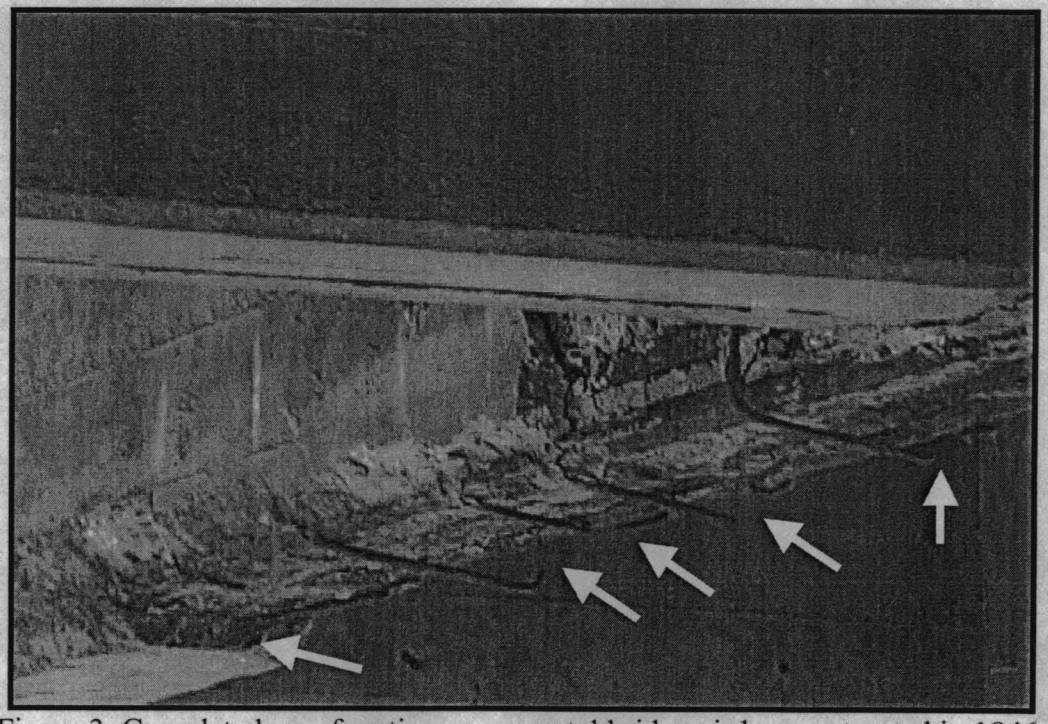

Figure 3: Complete loss of section on a coastal bridge girder constructed in 1946.

3.0 Specimen Design

Beam specimens in this study were designed to reflect 1950's era proportions and details. A survey of several 1950's CRC bridges and review of pertinent AASHTO codes of the time were conducted to obtain reasonable and representative design parameters. Design parameters were chosen to represent cross-sectional properties at a shear-critical section, a distance that is half of the effective depth (d/2) from the support for both simply supported spans and continuous spans. The design parameters used to select the cross-sectional properties were area of flexural steel relative to concrete shear contribution (A_s/V_c), the reinforcement ratio (ρ), area of compression steel relative to concrete shear contribution (A'_s/V_c), compression steel reinforcement ratio (ρ'), shear force carried by stirrups relative to the concrete shear contribution (V_s/V_c), and nominal shear resistance relative to the nominal moment capacity ($(V_s+V_c)/M_n$). The concrete shear resistance V_c was taken equal to $2\sqrt{f'_c}$ as permitted by the AASHTO Standard Specification 6th Edition (AASHTO, 1953). The design parameters considered are shown in Table 1. Based on these parameters, a specimen cross-section was designed with an effective width of 10-in, overall height of 24-in, effective depth of 20.5-in, and $\rho = 1.9\%$. The overall length of the beam was chosen as 10-ft with an 8-ft clear distance between supports. The span to effective depth ratio (a/d) was equal to 2.04. This value was chosen so that shear would

dominate response and provide a shear span with a manageable number of stirrups to corrode.

Design Parameters	Simply Supported Span			Continuous Span		
	min.	average	max.	min.	average	max.
A_s / V_c	9.8%	**16.07%**	22.9%	14.4%	**15.5%**	16.7%
ρ	1.14%	**1.88%**	2.63%	1.7%	**2.35%**	3.0%
A'_s / V_c	0.65%	**1.22%**	2.1%	3.6%	**4.87%**	6.6%
ρ'	0.07%	**0.14%**	0.22%	0.39%	**0.9%**	1.82%
V_s / V_c	70.2%	**152.2%**	193.5%	48.8%	**103.3%**	145%
$V_s + V_s / M_n$	7.3%	**9.57%**	10.9%	5.9%	**10.8%**	18.9%

Table 1: Specimen Design Parameters

Three different cross sectional shapes were tested as shown in Figure 4. Specimen Type I was a rectangular cross-section and was used to study the influence of stirrup spacings of 8, 10, and 12-inches. Section Types II/III included a deck slab. The effective width of the deck (b_e) was determined using the 6th Edition AASHTO Standard Specification (AASHTO, 1953) and was controlled by the span length (L/4). Type I and II specimens reflect shear in the positive moment region of a beam, while the Type III specimens reflect shear in the negative moment region, such as at continuous support locations as illustrated in Figure 5. Specimen Types II and III were all constructed with 10-inch stirrup spacing only. All beams have the bottom layer of flexural steel anchored using a standard hook to prevent pull-out failure of the tension steel. Flexural steel was epoxy-coated to isolate corrosion to the stirrups within the test span. The stirrups within the test section were plain black reinforcing bars with epoxy applied to the top bend locations where an electrical connection was made. This was done to prevent corrosion and preclude anchorage failure of the stirrup at the top of the beam.

Stirrups within the uncorroded portion of the specimen were epoxy coated and spaced at 6-in to force failure in the test span. Beams were identified with a number and letter designation: the first number indicating stirrup spacing, a letter corresponding to the cross sectional geometry and a final letter corresponding to the corrosion damage state. For example, Specimen 10RA was a rectangular section with 10-inch stirrup spacing and a damage state of A.

The concrete mix design was intended to represent a vintage 1950's 3000-psi mix and contained no admixtures. Mix proportions are shown in Table 3 and were provided by a local ready-mix supplier. Chlorides were added to the mix using reagent grade sodium chloride (NaCl) that was dissolved in water and then added to the concrete. The amount of NaCl added was 8.24 lb/yd^3 to obtain a Cl^- level of 5 lb/yd^3. Specimens were cast from three batches, wet cured for a period of seven days, and then permitted to dry cure for a period of 28-days. After at least 28-days of curing, the accelerated corrosion process was started. The 28-day curing permitted the concrete to achieve the design strength, so corrosion cracking would be representative of field conditions and not be influenced by time varying concrete strength.

Beam Type	Beam Dimensions												
	h [in]	b [in]	b_w [in]	d [in]	ρ [%]	A_s [in^2]	f_y [ksi]	d' [in]	A'_s [in^2]	f'_y [ksi]	s [in]	A_v [in^2]	f_{yv} [ksi]
I		10		20.5	1.9				1.7		8,10,12		
II	24	24	10	20.5	1.9	3.95	72	2.5	1.2	70	10	0.4	64
III		24		21.5	1.8				1.7		10		

Table 2: Beam cross-sectional properties.

Type I Cement	520	lb/yd^3
Water	300	lb/yd^3
3/4 Coarse Aggregate	1730	lb/yd^3
Fine Aggregate	1364	lb/yd^3
Reagent Grade NaCl	8.24	lb/yd^3

Table 3: Concrete Mix Design

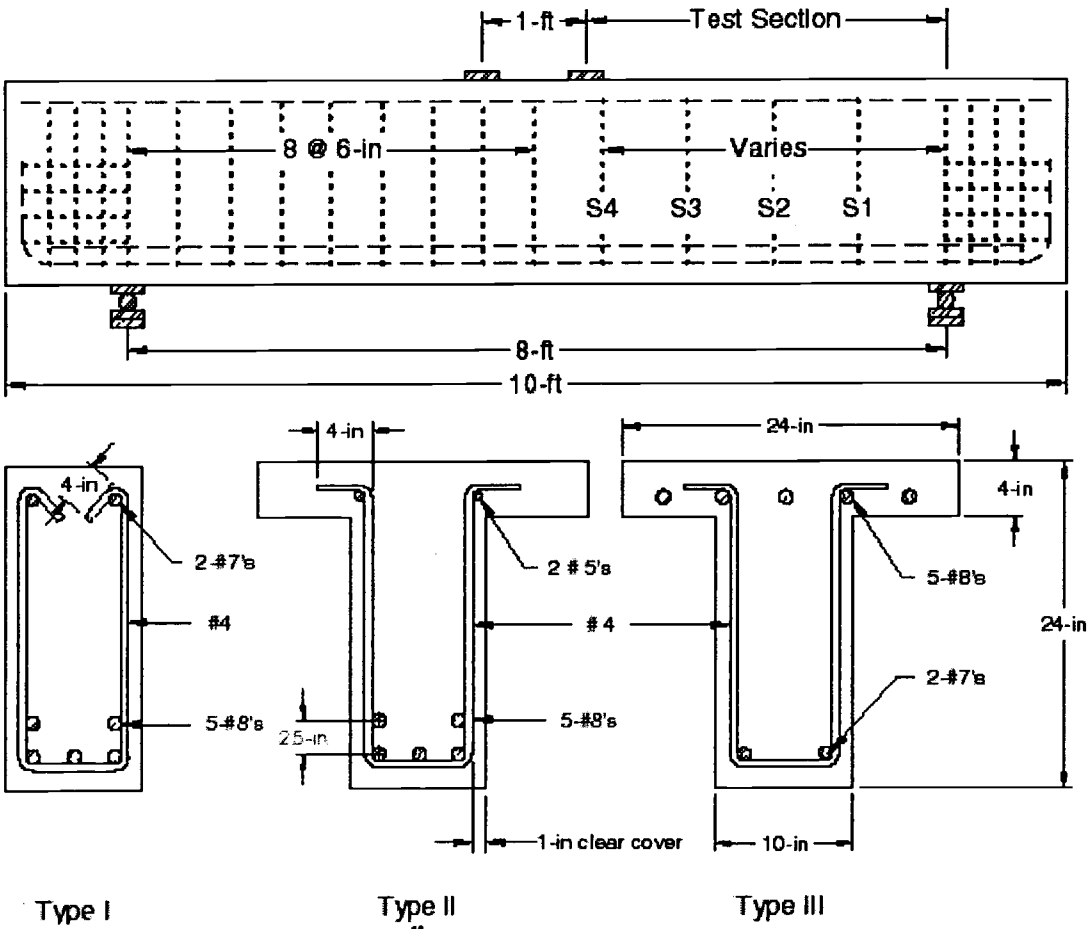

Figure 4: Specimen cross-sections.

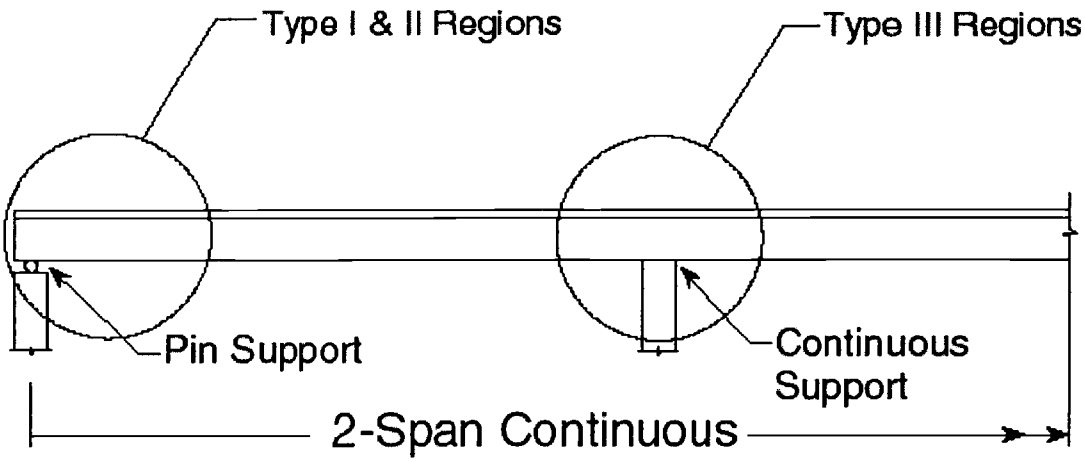

Figure 5: Cross-section designation.

4.0 Experimental Program

4.1 Accelerated Corrosion of Stirrups

After curing, specimens were subjected to accelerated corrosion. The 10R series was corroded to achieve four damage states. The 8R and 12R series were tested at two damage states. Series 10T and 10IT were tested at three damage states. State A corresponds to a beam with no corrosion damage. Damage state B (Light) corresponds to an approximate average nominal section loss of 12%. Damage state C (Moderate) corresponds to an approximate average section loss of 20%. The final damage state, D (Severe), corresponds to a nominal average section loss of approximately 40%. Specimens and their corresponding corrosion damage states are summarized in Table 4.

Beam	Cross Section	Stirrup Spacing	Corrosion Level
8RA	I	8	None
10RA	I	10	None
12RA	I	12	None
10TA	II	10	None
10ITA	III	10	None
10RB	I	10	Light
10RC	I	10	Moderate
10TC	II	10	Moderate
10ITC	III	10	Moderate
8RD	I	8	Severe
10RD	I	10	Severe
12RD	I	12	Severe
10TD	II	10	Severe
10ITD	III	10	Severe

Table 4: Specimen Designation

The accelerated corrosion process was conducted using a corrosion cell to pass current through the stirrups within the test span. The corrosion cell consisted of a 14 gauge galvanized wire mesh with 1/4-inch spacing in both directions acting as the cathode, and placed on the sides and bottom of the beams. The stirrups, #4 rebar, acted as the anode and were connected in series to a current supply. A wetted cotton towel was placed between the galvanized wire mesh and the concrete surface to provide electrical contact and to maintain low resistivity of the concrete. The cotton towel also allowed oxygen to diffuse to the concrete. Automated pumps circulated water over the specimen to maintain wetting and drying cycles. A schematic of the corrosion cell is shown in Figure 6. Current was impressed through the stirrups at a constant current density of 9.83-mA/in^3. The current passing through the stirrups was updated daily to maintain the current density even as the bar area was reduced due to corrosion, the prediction of the corrosion rate is shown in Figure 7. The current density was sufficiently high so as to provide a reasonably fast corrosion time.

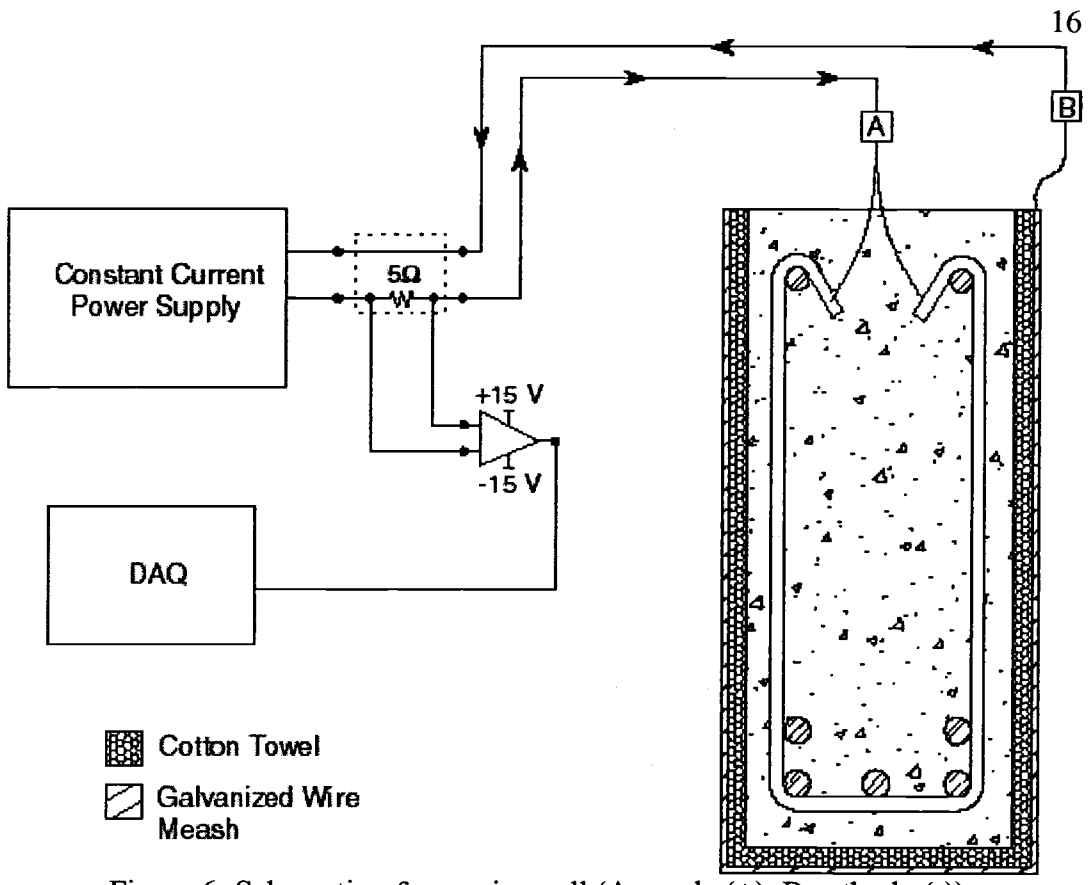

Figure 6: Schematic of corrosion cell (A-anode (+), B-cathode (-)).

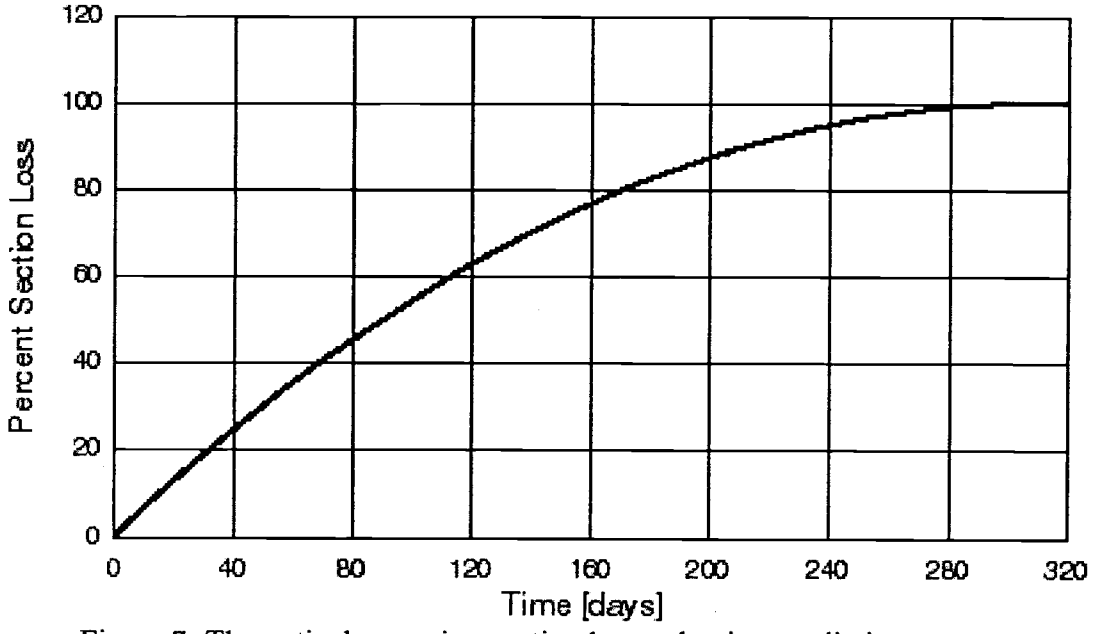

Figure 7: Theoretical corrosion section loss reduction prediction curve.

The current required for the stirrups and the section loss were determined using Faraday's Law for a cylinder. The applied current was determined as follows:

$$I_t = i_{desired} 2\pi L r_{t-1} \quad [4]$$

where I_t is the applied current [mA], $i_{desired}$ is the current density [mA/in^2]' L is the exposed rebar length [in.], r_{t-1} is the old rebar radius [in.] at time t-1. From Eq 4 the actual current density at time t [hr.] was calculated as follows:

$$i_t = \frac{I_t}{2\pi L r_{t-i}} \quad [5]$$

the new radius, r_i, was calculated by:

$$r_t = r_{t-1} - 8.0856x10^{-6} i_t (t_i - t_{i-1}) \quad [6]$$

where t_i is the new time. The section loss was then calculated at time t as follows:

$$\%SL = 100\frac{r_o^2 - r_t^2}{r_o^2} \quad [7]$$

where r_o is the original radius of the stirrup measured using the whole length of the bar. A data acquisition program was written to automatically calculate and update results of Equations [4] to [7] to provide the required current.

4.2 Visual Damage Assessment

During the accelerated corrosion process, cracks produced from corrosion were mapped and recorded. Areas of delaminations and spalls were also recorded. Prior to testing, all beams were given a final inspection and were

rated according to Oregon Department of Transportation and federal inspection guidelines. All rating information was taken from the Oregon Department of Transportation Bridge Inspection Pocket Coding Guide (ODOT, 2001). To ensure the specimen rating was consistent to field practice, ODOT inspection personnel provided independent ratings for initial specimens. The items that were rated for this study relate to beam elements only and included: Item #12 "Concrete Deck-bare", Item #110 "Open Girder/Beam", Smart Flag #358 "Deck Cracking", Smart Flag #359 "Soffit Cracking". A description of these elements and the range of rating values are shown in Table 5. All elements, except for Item #12, are assigned a number and then percentage that represents the area affected. Item #12 is only rated with a number. For example, a beam with severe damage on only half of the span would be rated for Item #110 as: 4-50%.

Item	Description	Rating			
		Best		Worst	
#12	Concrete Deck-bare	1	Little/No Damage	5	Significant Damage
#110	Open Girder/Beam	1	Little/No Damage	4	Advanced Deterioration
#358	Deck Cracking	1	Deck Cracked	4	Large Unsealed Cracks
#359	Soffit Cracking	1	Little/No Cracking	4	Severe Rust Stainging/Spalling
59	Superstructure	9	Excellent Condition	0	Failed Condition

Table 5: Description of Inspection Rating Items (ODOT, 2001).

4.3 Structural Test Setup

Once beams reached the desired corrosion damage state, they were removed from the corrosion cell and tested to failure. Beams were tested in a four-point loading configuration with the load applied through a spreader beam. Load application points near the center of the specimen were spaced

12-inches apart. Load was measured with a 300-kip capacity load cell placed between the spreader beam and hydraulic cylinder. Displacement at midspan of the beam was measured at middepth of the section. Deformation of the supports was measured using displacement transducers placed on top of the support plates. Support deformations were then subtracted from the midpsan displacement to determine the specimen deformation. Rotations were measured using bi-axial tilt sensors located at supports. Concrete stresses were measured using clip-gages at two locations: the compressive face at midspan between the load points, and diagonal concrete stress within the corrosion test span. Strain gages were placed at midspan on the longitudinal steel on one side of the beam face. Strain gages were also placed on the stirrups at midheight for all "A" specimens. Crack widths were measured three ways: displacement transducers were placed in the test span on diagonals to measure total deformation in the section, small displacement transducers were mounted across shear cracks after formation, and at each load step after formation of shear cracking with a visual crack comparator. The test setup and instrumentation placement is shown in Figure 8. Loading progressed with two initial cycles from 0 to 10-kips to ensure data was being properly acquired. After verification of data collection, the load was increased monotonically until failure. Loading was suspended at 25-kips intervals to mark and measure cracks.

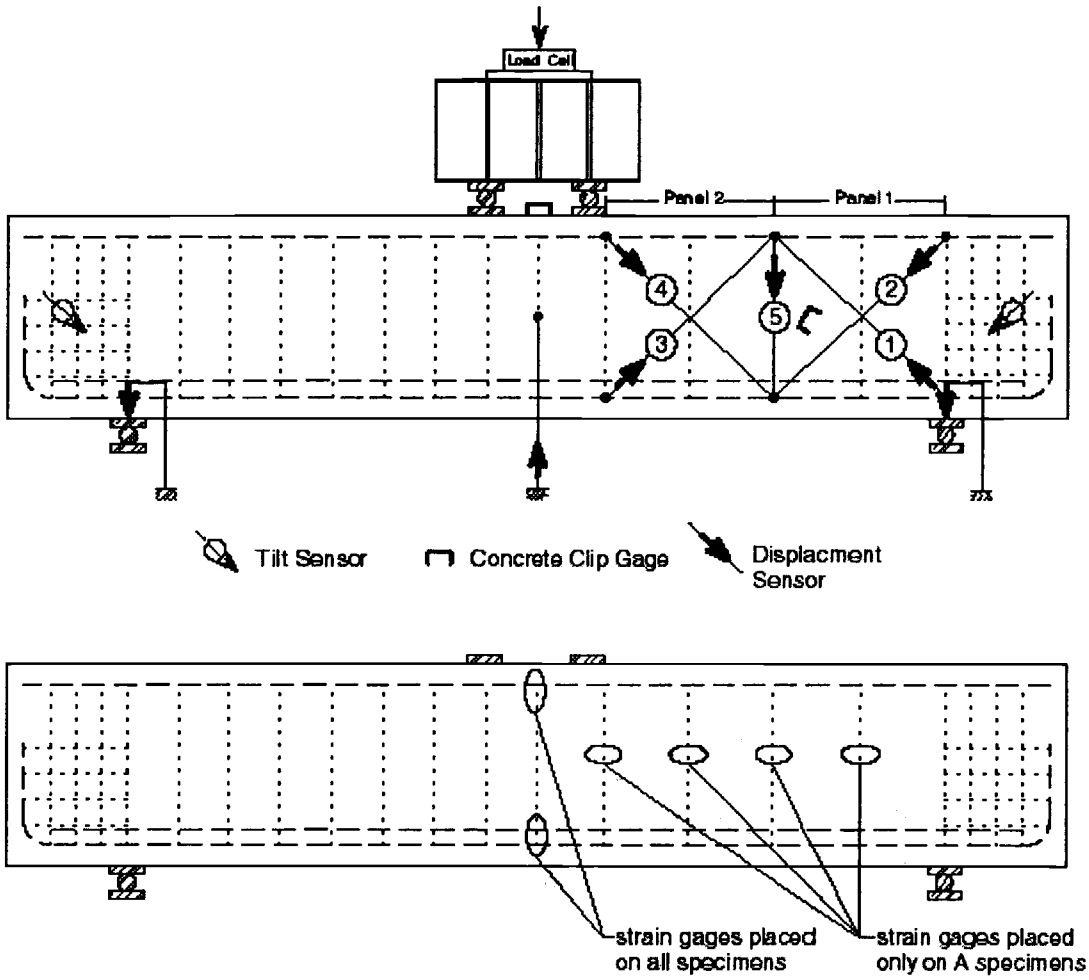

Figure 8: Test Setup

4.4 Rebar Section Loss Measurement

After testing, stirrups that were located in the failure region were removed from the beams to determine the actual amount of section loss and extent of corrosion damage. After removal from the beams, the stirrups legs were cut into manageable pieces (a length of about 16-in) and cleaned in accordance with ASTM G1-99 (2001). The corrosion damage was quantified to determine both average and local maximum cross-sectional area loss. Average section loss was determined by the gravimetric method. The gravimetric method determines the volume of the bar by weighing the specimen in air and then in water, the difference divided by the specific gravity of water is the volume of the specimen. The area is then determined by dividing by the length of the specimen. Local maximum section loss was determined using a contour gage. The contour gage is used to determine that local area by using the gage to get the contour of the specimen and then transferring the measured contour to graph paper where the area can be determined. This method was used over vernier calipers based on the fact that the calipers do not accurately determine the area of a bar that has localized corrosion.

5.0 Test Results and Discussion

5.1 Corrosion Damage Assessment

Based on visual inspection, initial cracking due to corrosion was determined. The amount of section loss at initial cracking was estimated from the theoretical section loss by Equation 7. The mean of all specimens indicated initial cracking at a nominal average section loss of 2.9%, and was not dependent on the concrete compressive strength. This is shown by looking at 12RD and the 10R series; even though the stirrups spacing was closer for the 12RD beam the beam cracked at a lower section loss level even though the concrete strength of the 12RD was less than the 10R series by 1000-psi. However, the percent section loss at first cracking did vary with stirrup spacing. Closer spaced stirrups produced cracking at smaller section loss (8RD at 1.8%, 12RD at 3.5%). The nominal percent section loss and calculate radius reduction at first cracking for all specimens are shown in Table 6.

Beam	f'_c [psi] 28-day	Initial Cracking	
		% Section Loss	Radius Loss [mils]
8RD	3950	1.8	2.3
10RB	4950	3.0	3.8
10RC		3.3	4.2
10RD		3.1	3.9
12RD	3950	3.5	4.5
10TC	5050	3.0	3.8
10TD		2.1	2.7
10ITC	4950	2.9	3.7
10ITD		3.1	3.9

Table 6: Section loss at first cracking

The observed corrosion cracking patterns were consistent for all specimens. Initially, cracks occurred in the fascia of the beam, and then propagated to the top and bottom of the beam. As the initial cracks grew, additional cracking occurred around the stirrups forming a triangular or wedge shaped incipient spall. A longitudinal crack propagated at or near the location of the longitudinal steel although the flexural steel was not corroding. Typical cracking and delaminations patterns are shown in Figure 9 at the severe damage state D. The widest corrosion crack recorded prior to structural testing was 0.04-inches.

While there was significant section loss, extensive cover cracking, delaminations, and rust staining, no major spalling occurred. It was expected that the concrete cover would fall away from the concrete, particularly at higher damage states. Sounding of the concrete was regularly conducted by tapping the surface with a hammer. Significant areas of delaminations were noted and some small areas of spalling were observed, but there were sufficient areas of contact to keep the cracked concrete cover attached to the beam. It is anticipated that the concrete cover would tend to spall under live loading, which would vibrate the structure and shake off loose concrete pieces. Following structural testing, the specimens were dissected and corroded stirrups were removed to analyze the degree of corrosion. The amount of concrete damage based on the extent of rust staining indicated significant loss of bond between the stirrups and concrete. Damage to the concrete from

corrosion was confined to the cover regions. Based on the visual distress after the tests, it is believed that the lack of anticipated spalling did not alter the performance of the beams because the cover concrete was delaminated and the effect of the corrosion cracking was noticeable after failure of the beam.

Powder samples of concrete were taken from 28-day cylinders and the "A" specimens in order to determine the actual chloride content of the concrete in accordance with AASHTO T260-94 (1994). The values were averaged to describe the chloride contents of the other beams. Individual beam samples from the corrosion series were not used because during the wetting and drying cycles, chlorides could be introduced to or leached from the beams. Summary results of the sample chloride contents can be found in Table 7.

Type	Corrosion Damage	Chloride Content [lb/yd^3]
8R	A	5.3
	D	
10R	A	4.3
	B	
	C	
	D	
12R	A	5.3
	D	
10T	A	6.2
	C	
	D	
10IT	A	5.3
	C	4.3
	D	

Table 7: Summary of chloride contents for specimens

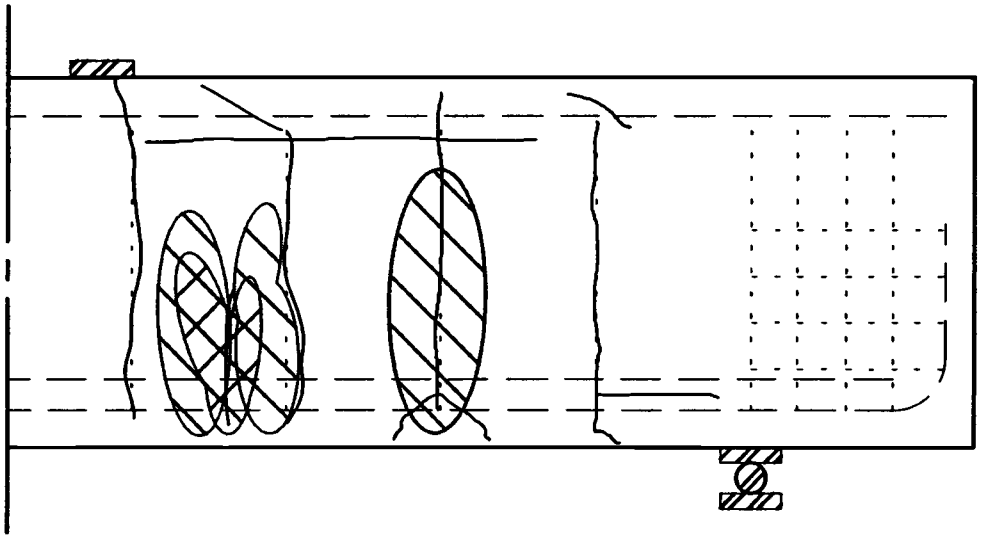

Figure 9: Typical corrosion crack pattern for 10R Series.
Delaminations Spall

The ratings of the beams were fairly consistent between the different beam series. Even though it was known from monitoring the current passing through each stirrup that the specimens had undergone significant corrosion damage, the rating values of the specimens were not severe. The lowest NBI Item #59 rating that was given was a 4/3. This specimen, 10ITD, had areas of spalling with significant delaminations and severe rust staining. Most of the corroded beams were given an Item #59 rating of 5 or 4. The other significant rating characteristic was for Item #110. For all specimens, rating was 3-100%, meaning evidence of corrosion was present on the test section. The ratings for all of the specimens can be found in Table 8.

Beam	Condition Assessment				
	# 12	# 110	# 358	# 359	NBI (Item 59)
8RA	NA	1-100%	NA	NA	9
8RD	NA	3-100%	NA	NA	4
10RA	NA	1-100%	NA	NA	9
10RB	NA	3-100%	NA	NA	5
10RC	NA	3-100%	NA	NA	5/4
10RD	NA	3-100%	NA	NA	4
12RA	NA	1-100%	NA	NA	9
12RD	NA	3-100%	NA	NA	4
10TA	1	1-100%	1-100%	1-100%	9
10TC	2	3-100%	1-50%	2-50%	5
10TD	2	3-100%	2-50%	4-50%	5
10ITA	1	1-100%	1-100%	1-100%	9
10ITC	2	3-100%	2-50%	3-100%	4
10ITD	3	3-100%	1-25%	5-100%	4/3

Table 8: Summary of NBI / ODOT inspection ratings

5.2 Structural Performance

5.2.1 Rectangular Series

Load-displacement responses for the rectangular beams with 8-in stirrup spacing are shown in Figure 10. Specimen 8RD was subject to severe corrosion damage and showed a capacity loss of 20% and a loss of ductility of 37% compared to the uncorroded specimen. The maximum load was obtained just prior to fracture of stirrup S2. Stirrup fracture occurred at the bottom bend location due to severe section loss. The largest shear crack width measured on the beam web prior to failure was 0.02 inches. The cracking patterns for the two beams at failure are shown in Figure 11, with the heavier line weight representing the failure crack. After failure, the stirrups crossing the failure crack (3 stirrups) were removed to determine the average and maximum local section loss. The average section loss was 29%, and is defined as average section loss of all stirrups that cross the failure crack. The maximum section loss was 64% and is defined as the maximum section loss of all stirrups in the failure region regardless of where it occurs on the stirrup leg. Section loss measurements for all removed stirrups (S1, S2, S3) are shown in Table 11. The concrete was also examined to assess the damage. Corrosion damage could be discerned from load induced damage based on rust staining. The close spacing of the stirrups caused

cover cracking from corrosion at individual stirrups to overlap, and a majority of the side cover was delaminated. This reduced the effective width of the beam. The total deformations along the diagonals that cross shear cracks within the two instrumented regions are shown in Figures 12 and 13. The figures show that the corroded beam cracked in shear at a higher load than that of the pristine specimen. Specimen 8RA showed no signs of shear cracking in panel 2 until just before failure. The behaviors in terms of total deformation for panels 1 and 2, for 8RD, were similar.

The load-displacement behaviors for rectangular beams with 10 inch stirrup spacing are shown in Figure 14. The four beams in this series showed a continual decrease in capacity with the higher damage states. The beams not only lost strength capacity but ductility as well. The loss in capacity for the corroded beams was 12%, 19%, and 30% for specimens 10RB, 10RC, and 10RD, respectively. The ductility loss for this series was 21%, 36%, and 33%, respectively, for damage states B, C, and D. The maximum load for specimens 10RA and B were obtained before the beams failed due to shear-compression failure of the concrete. The maximum load for 10RC and D were obtained prior to fracture of stirrup S2 and S3, respectively. The stirrup in 10RC fractured at a point above the flexural steel due to severe section loss. The

maximum crack width measured prior to failure was 0.025 inches and occurred at the location of the bar fracture. Stirrup S3 in 10RD fractured at point of severe section loss at a point below the compression steel. Crack maps for the 10R Series are presented in Figure 15, with the heavier line representing the failure crack. After failure, the stirrups that crossed the critical crack (2 stirrups) were removed to determine the average and local maximum section loss. The average of the 2 stirrups in the critical region for specimen 10RB is 13%, while the local maximum was 34%. For specimen 10RC the average section loss was 23% and the local maximum was 61%. For the severely corrosion-damaged specimen, 10RD, the average section loss was 32% while the local maximum section loss was 100%. The section loss measurements for all stirrups for the 10R series are shown in Table 11. The concrete was examined after failure to assess damage from corrosion. The spacing of the stirrups was sufficient so that the corrosion cover cracking just overlapped and that wedge shaped pieces of side cover were delaminated. Measured crack widths did not vary significantly between different specimens in this series except for 10RC, where the maximum crack width occurred at a fractured stirrup location. The total deformation along the diagonals that cross the shear cracks is shown in Figures 16 and 17.

The total deformations continually decreased for specimens 10RA to 10RC. This trend changed for 10RD, where the cracks within both panels were quite wide. The crack widths tended to be wider than those observed for the undamaged specimen even though the severely damaged specimen fails at 30% less load.

The load-displacement behaviors for rectangular beams with 12-in stirrup spacing are shown in Figure 18. Specimen 12RD was subject to severe corrosion damage and showed a capacity loss of 10.5% and a loss of ductility of 18%. The maximum load was obtained just prior to fracture of stirrup S1. The stirrup fractured at the location of the shear crack. The maximum crack width measured prior to failure was 0.06 inches and occurred at the failure crack location where the stirrup was completely corroded away. Cracking patterns for the two beams of the series are shown in Figure 19. After failure, the stirrups (2) that were crossed by the critical crack were removed to determine the average and maximum local section loss (34% and 100%, respectively). The section loss measurements for all of the stirrups (S1, S2) are summarized in Table 11. The concrete was examined, and it seemed that the wide spacing of the stirrups prevented the corrosion cracking from overlapping. The concrete damage was small compared to the section loss of the stirrups, and stirrup S2 had complete section loss

on one leg and the beam was able to sustain the load until stirrup S1 fractured causing failure. The total deformations along the diagonals that cross the shear cracks within the two instrumented regions are shown in Figures 20 and 21. Specimen 12RD cracked at a higher load than the 12RA specimen. The maximum deformations for both panels were similar with only a small increase in panel 1 for the corroded specimen. Due to the widely spaced stirrups, the concrete contribution to shear capacity is somewhat larger for this series than the previous groups.

Overall, the performance of the rectangular series was dependent on stirrup spacing. The 8R and 10R series exhibited similar capacities. The remaining capacity for the severely damage (D) specimens for both of these series was 79% and 70%, respectively. The similar behavior of these two series can be attributed to the similar extents of corrosion damage that occurred to the concrete in the test span and the stirrup contribution to shear capacity. The cover cracking for both these series specimens was close enough to overlap and thus delaminations of significant portions of the concrete were produced. The severely corroded specimen with 12-inch stirrup spacing exhibited a capacity loss of only 10%. This small reduction was due to concrete cover damage

from the stirrup corrosion that did not overlap and the lower relative contribution to strength from the stirrups.

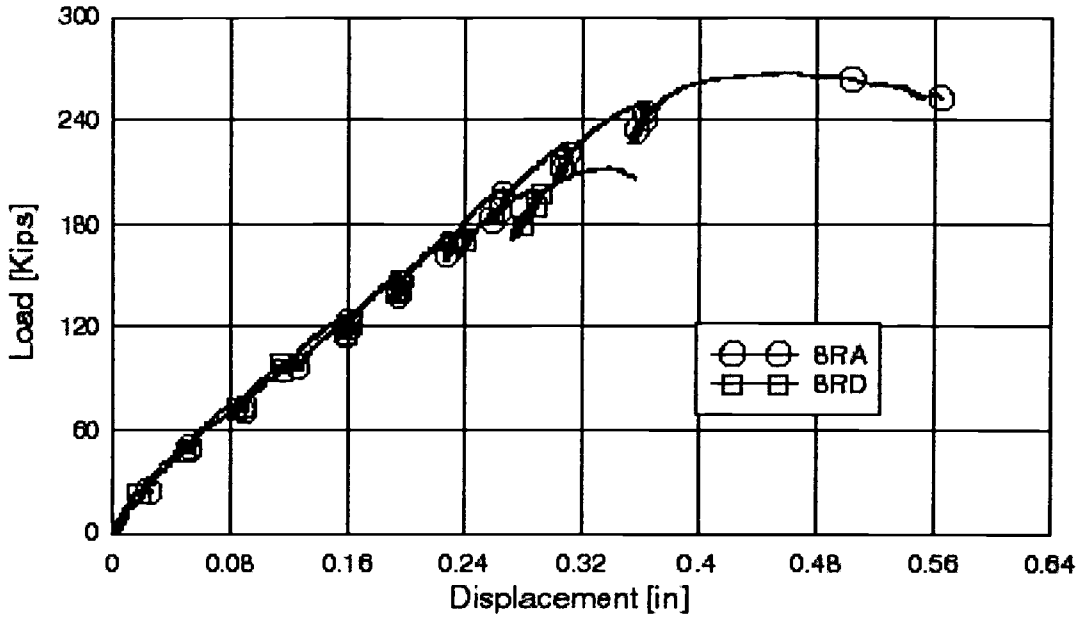

Figure 10: 8R Series load-displacement plots.

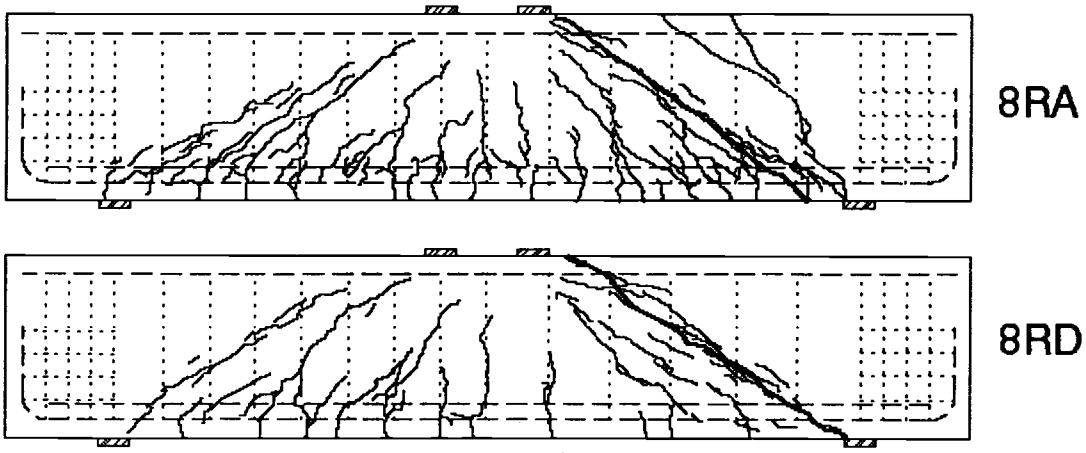

Figure 11: 8R Series crack maps.

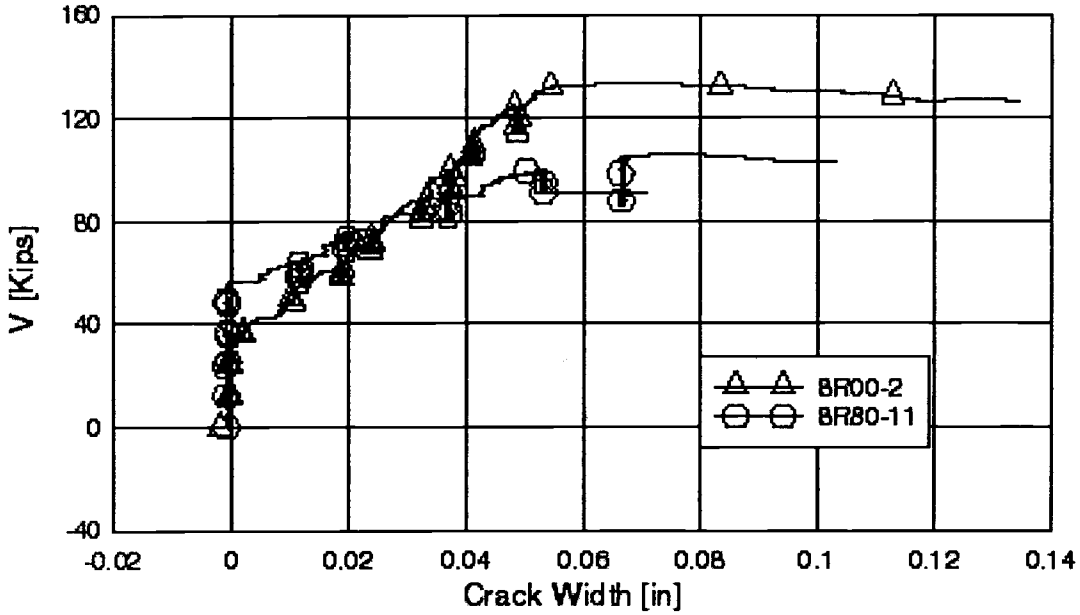

Figure 12: Deformations measured across cracks within Panel 1 for 8R Series

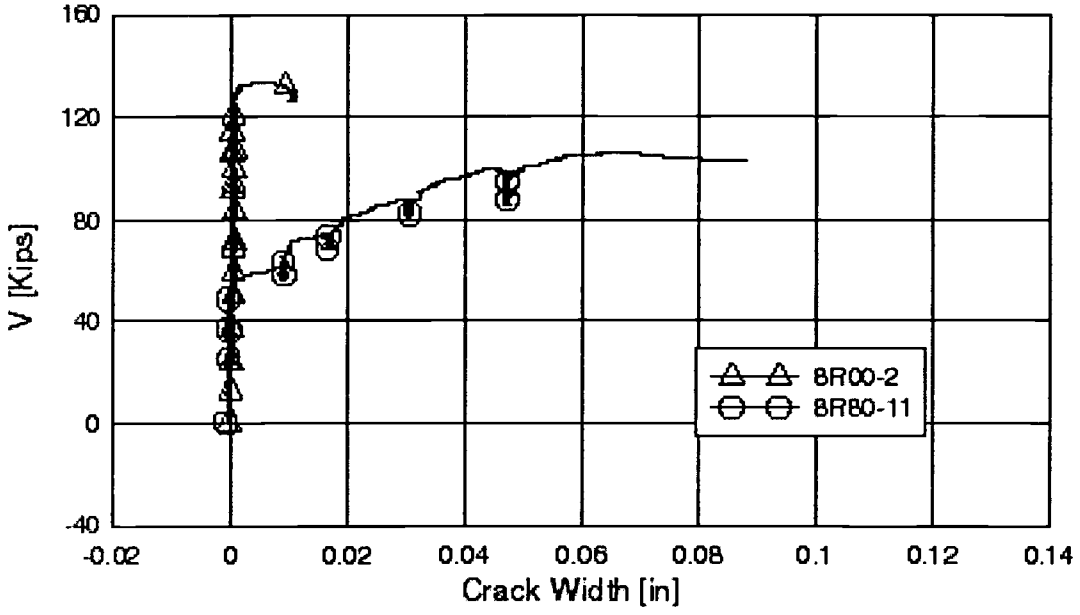

Figure 13: Deformations measured across cracks within Panel 2 for 8R Series

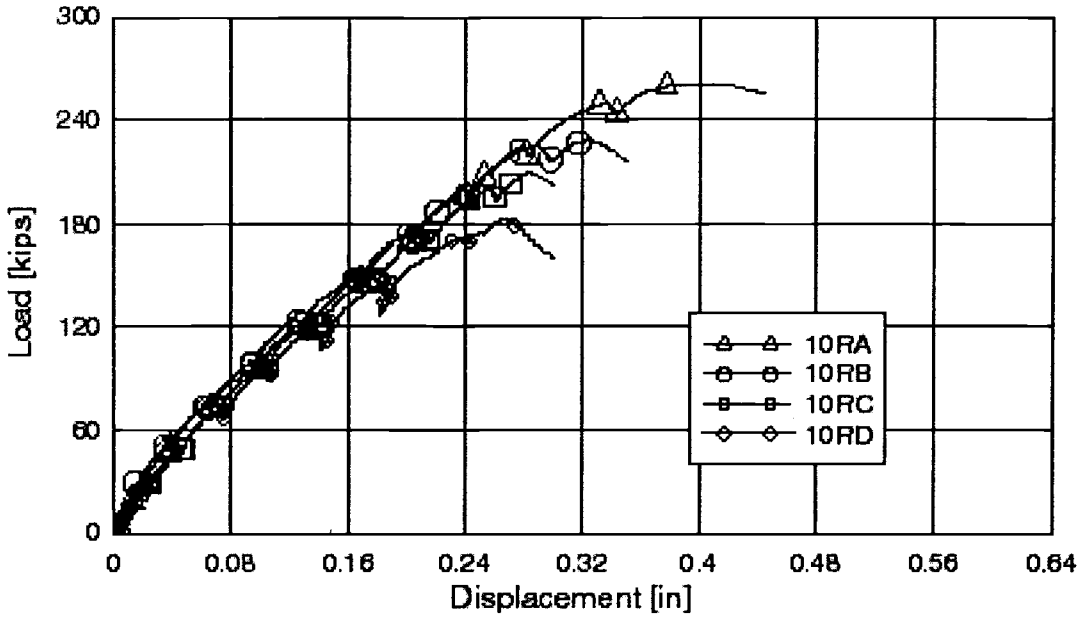

Figure 14: 10R Series load-displacement plots.

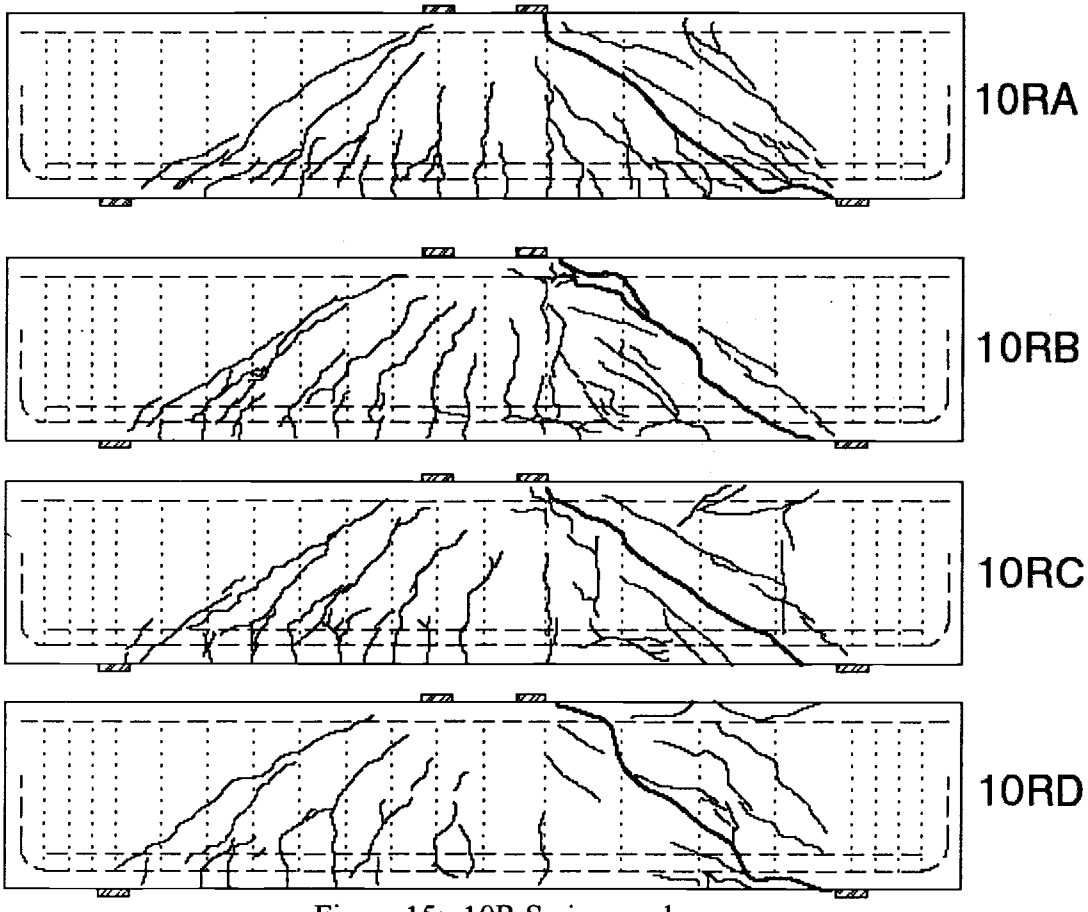

Figure 15: 10R Series crack maps.

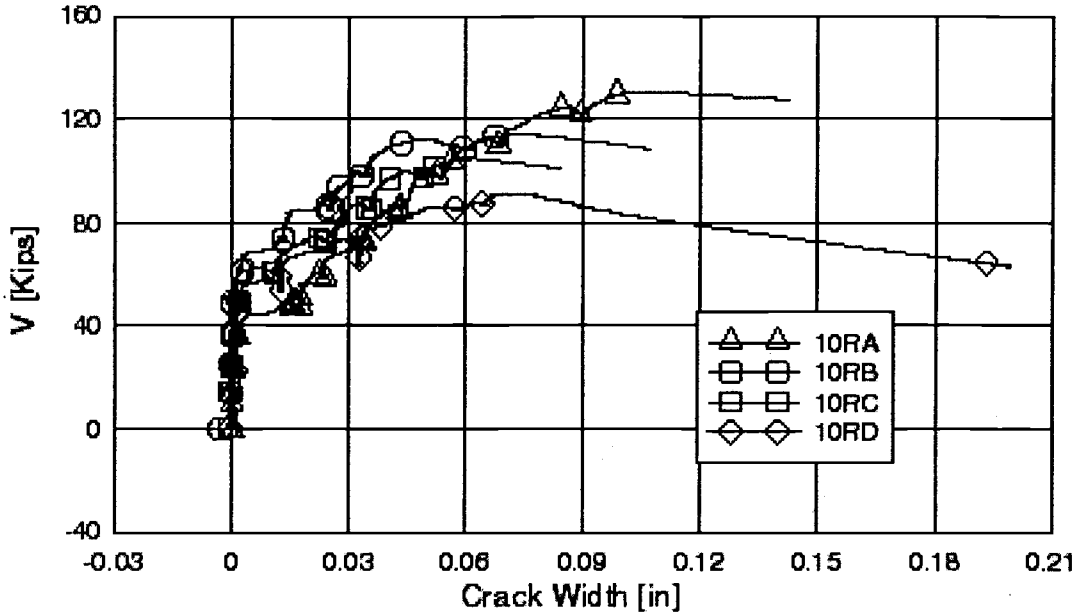

Figure 16: Deformations measured across cracks within Panel 1 for 10R Series.

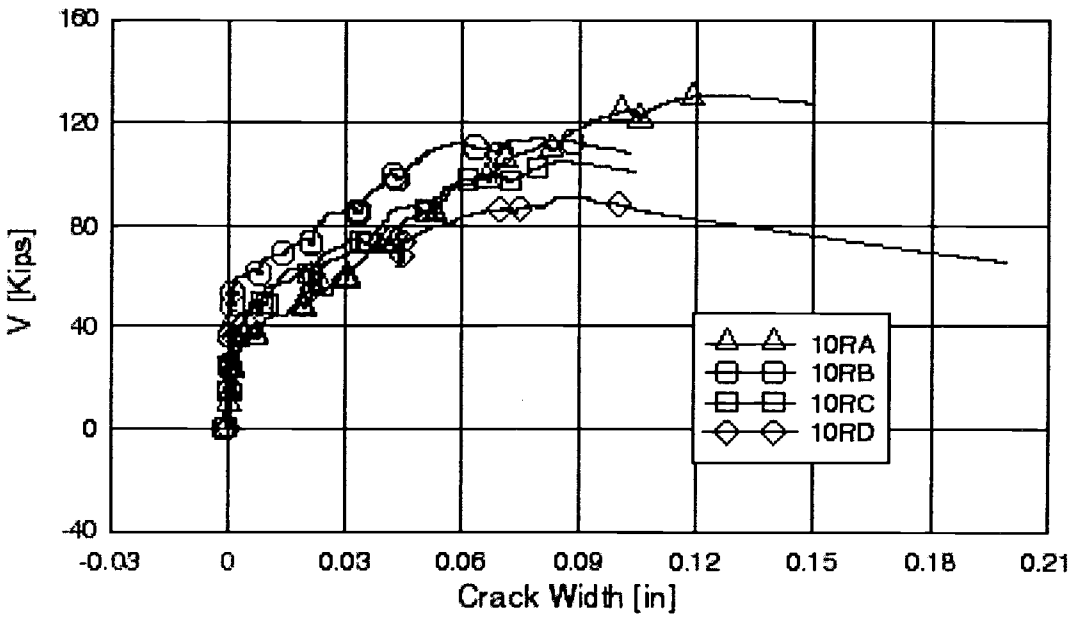

Figure 17: Deformations measured across cracks within Panel 2 for 10R Series

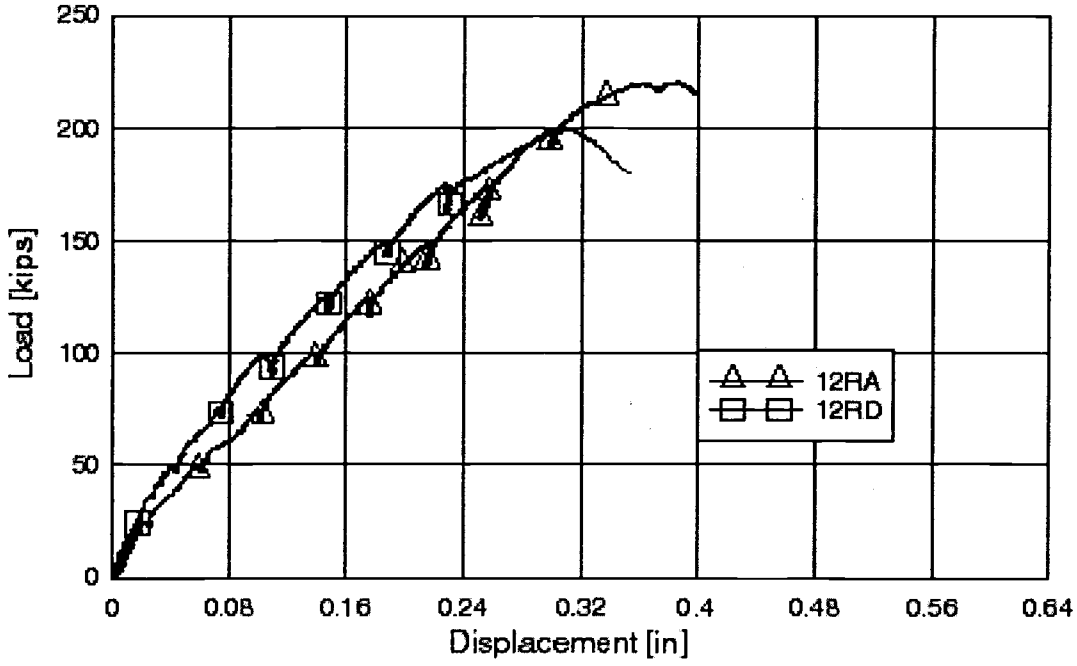

Figure 18: 12R Series load-displacement plots.

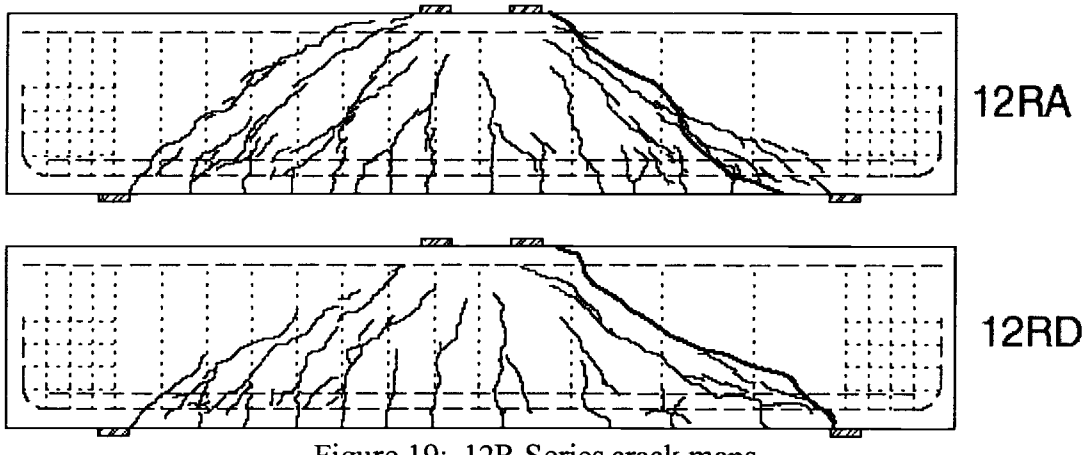

Figure 19: 12R Series crack maps.

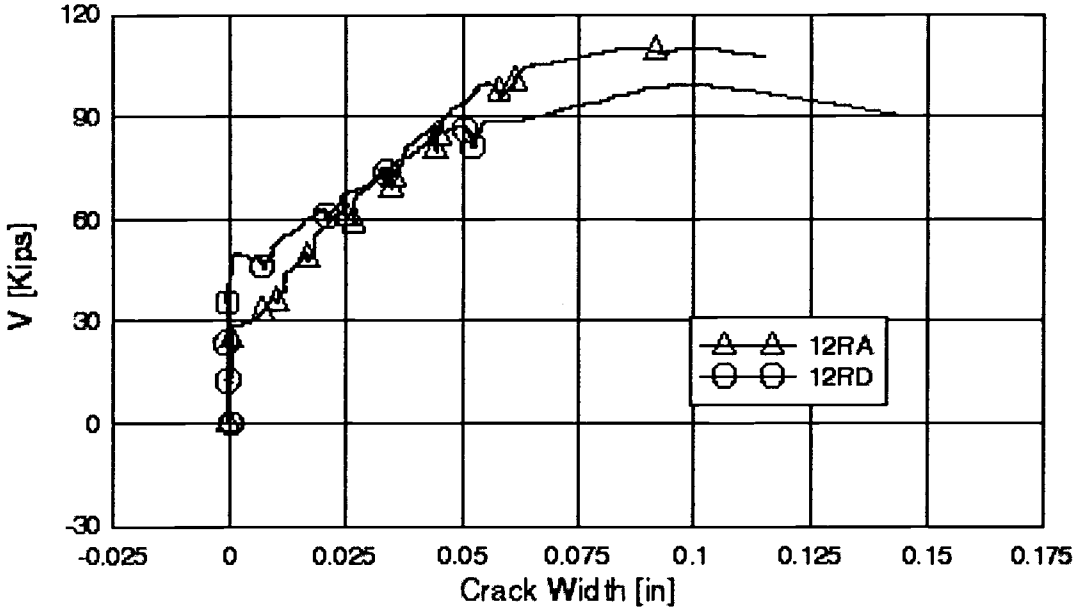

Figure 20: Deformations measured across cracks within Panel 1 for 12R Series.

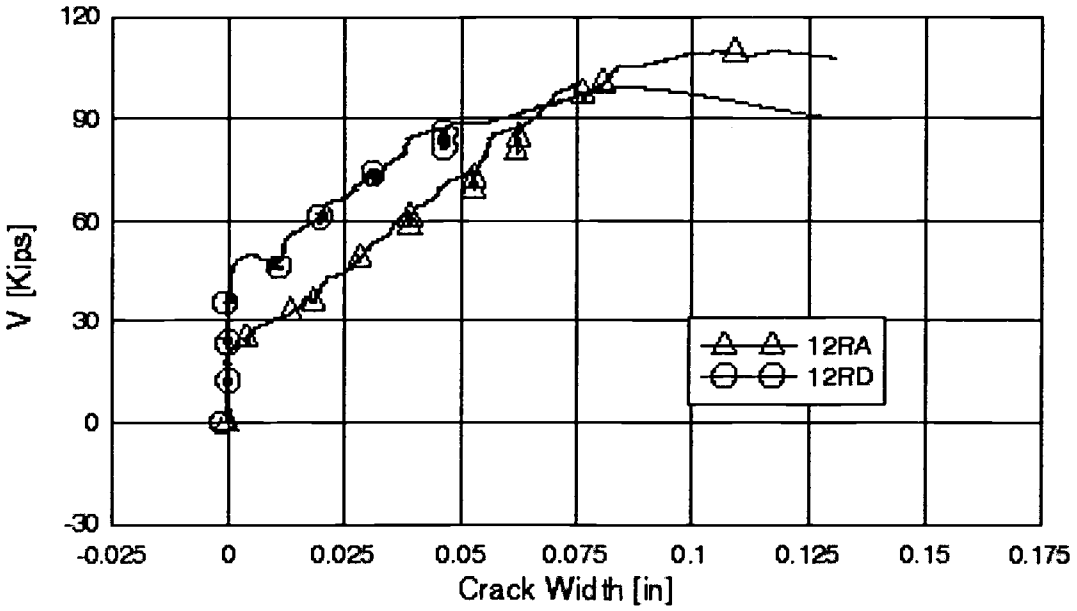

Figure 21: Deformations measured across cracks within Panel 2 for 12R Series.

5.2.4 10T Series

The load-displacement behaviors for T-beams with 10 inch stirrup spacing are shown in Figure 22. Specimen 10TC was subject to moderate corrosion damage and showed a capacity loss of 26% and a loss of ductility of 38%. The maximum load was achieved just prior to fracture of stirrup S2; prior to this, stirrup S1 had fractured. Stirrup S1 fractured at the bottom corner bend due to severe section loss from corrosion, while stirrup S2 fractured near the top layer of the flexural steel. The maximum crack width measured prior to failure was 0.04 inches. Specimen 10TD showed a capacity loss of 6% and showed no significant loss of ductility. Beam 10TD failed after fracturing stirrup S1 at the level of the top layer of flexural steel. Cracking patterns for the three beams of the series are shown in Figure 27. After failure, the stirrups that were crossed by the critical crack were removed to determine the average and maximum local section loss. The average and maximum section loss for 10TC was 20% and 73%, respectively. The severely corrosion-damaged specimen had an average section loss of 33% and a local maximum section loss of 100%. The section loss measurements for all of the removed stirrups are shown in Table 11. The corrosion damage that occurred to the concrete was similar to that for the 10R series. The

deck portion of the beams developed cracks from corrosion but no delaminations or spalling was observed. The capacity loss of the moderately damaged T-beam was greater than that of the severely damaged specimen due to the adverse locations of the maximum section loss on the stirrup legs. Even though stirrup S2 of specimen 10TD had undergone complete section loss, the critical crack crossed the stirrup at an area where there was relatively little section loss. Since both of the stirrups in 10TC had fractured due to severe section loss at areas where the critical crack crossed, the beam failed at a lower load. The total deformation along the diagonals that cross the shear cracks for the 10T Series did not change due to corrosion damage, as shown in Figures 24 and 25.

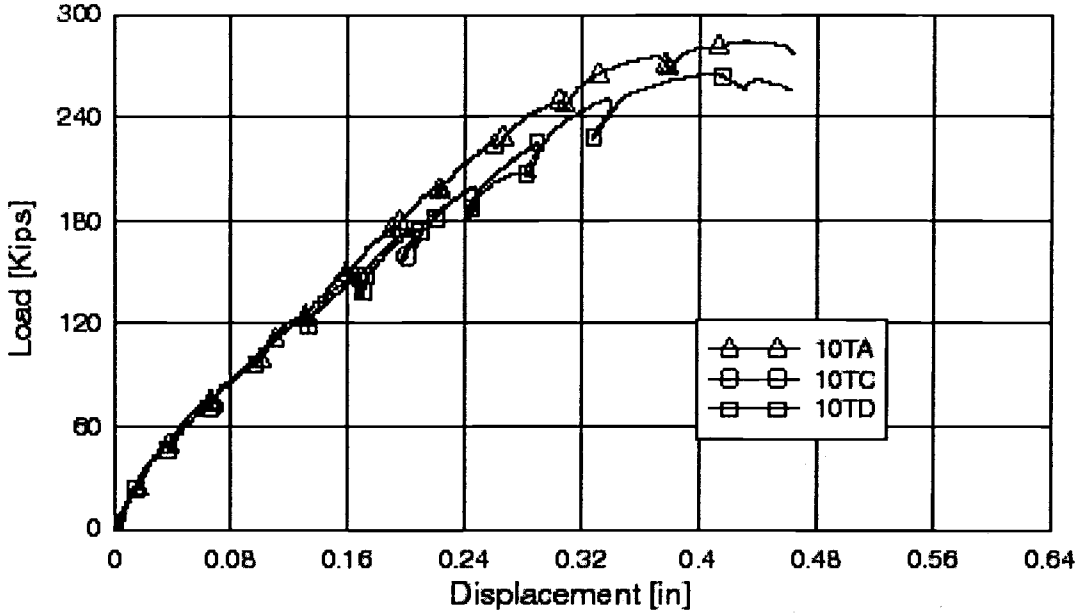

Figure 22: 10T Series load-displacement plots.

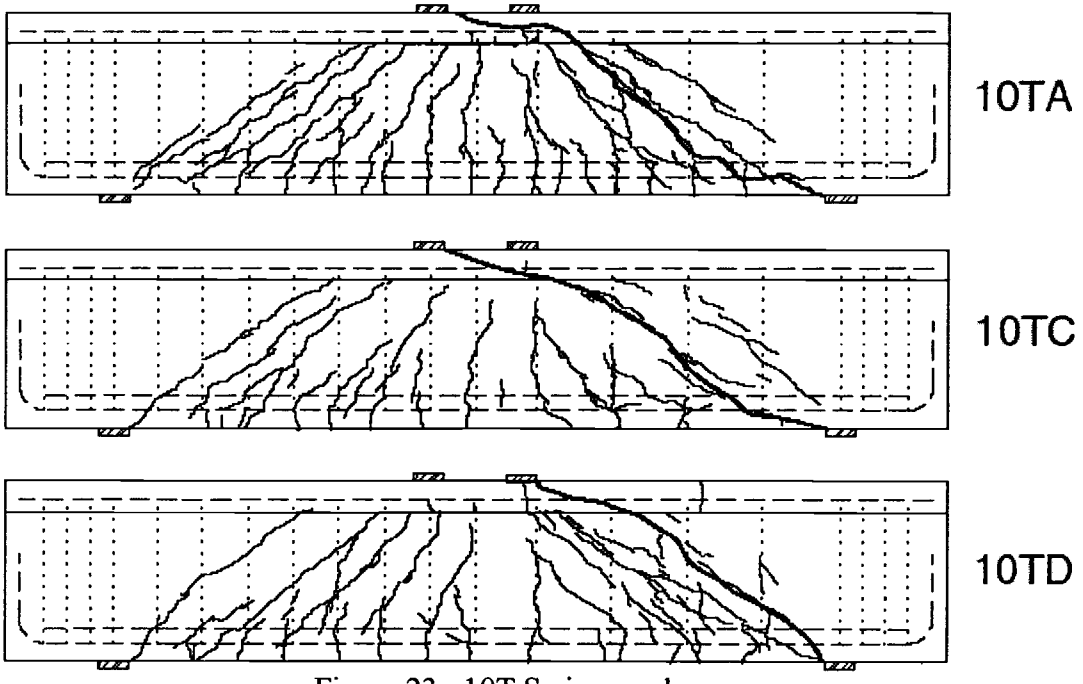

Figure 23: 10T Series crack maps.

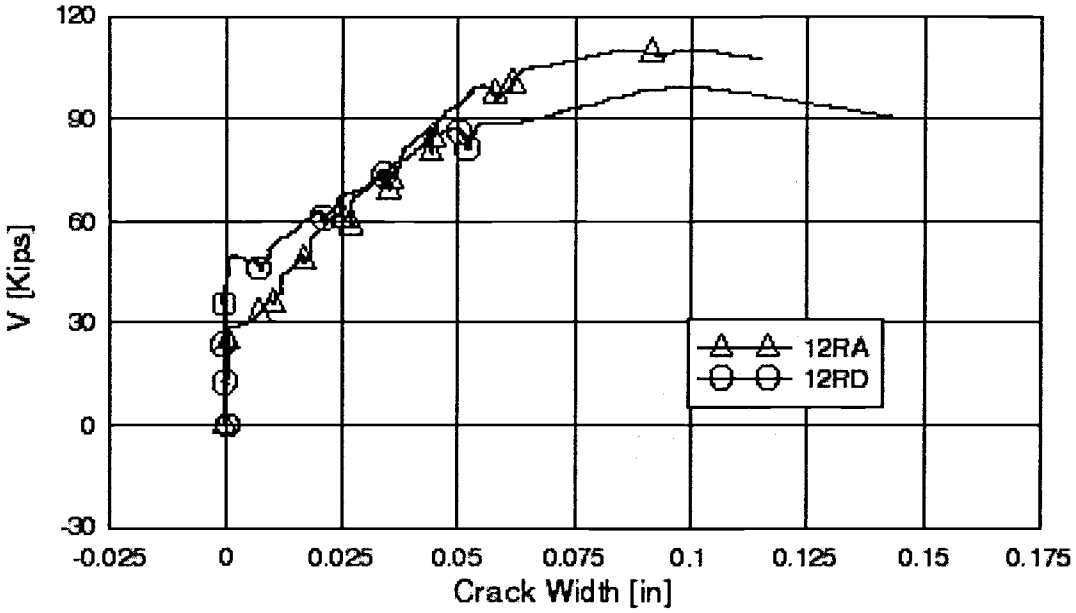

Figure 24: Deformations measured across cracks within Panel 1 for 10T Series.

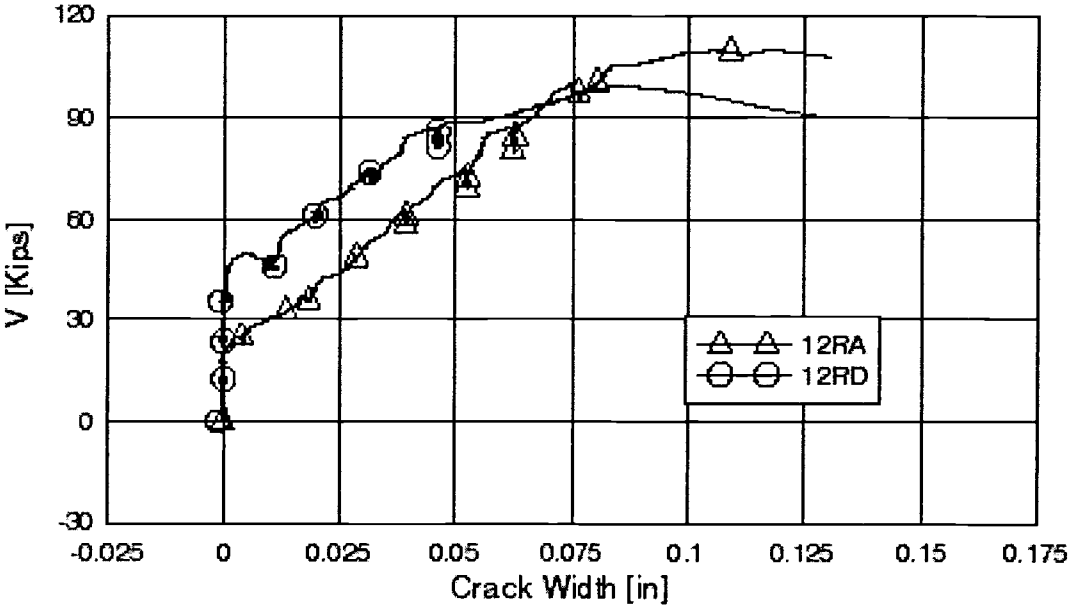

Figure 25: Deformations measured across cracks within Panel 2 for 10T Series.

5.2.5 10IT Series

The load-displacement behaviors for the inverted T-beams with 10 inch stirrup spacing are shown in Figure 26. Specimen 10ITC was subject to moderate corrosion damage and showed a capacity loss of 5% and a loss of ductility of 9%. Specimen 10ITC failed due to shear-compression failure of the concrete. The maximum crack width measured prior to failure was 0.025 inches. Specimen 10TD showed a capacity loss of 42% and a ductility loss of 24%. The beam failed upon fracture of stirrup S3. The stirrup fractured approximately 3 inches below the deck soffit. Cracking patterns for the three beams in the series are shown in Figure 27. Average and maximum section loss of the stirrups was measured for 10ITC at 17% and 20%, respectively. The severely corrosion-damaged specimen, 10ITD, had an average section loss of 36% and a local maximum section loss of 72%. The section losses measured for all removed stirrups are shown in Table 11. The corrosion damage that occurred from the concrete was again similar to that of the 10R series. The deck developed large cracks from corrosion but no delaminations or spalling was observed. Cracks formed on 10ITC and 10ITD along the flange web interface. The total deformations along the diagonals that cross the shear cracks for the 10IT Series are shown in Figures 28 and 29. The total deformation for the

inverted T-beams changed due to corrosion damage. The maximum crack width for the heavily corroded beam was less than that for the moderately damaged beam. Specimen 10ITD first showed signs of shear cracking that propagated quickly to failure.

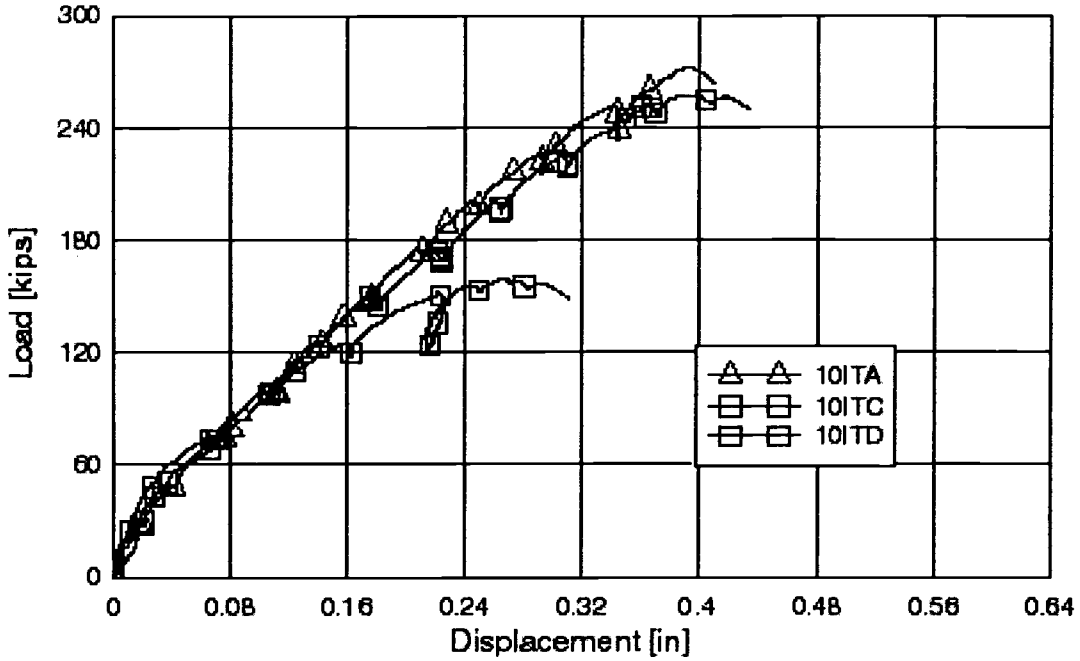

Figure 26: 10IT Series load-displacement plots.

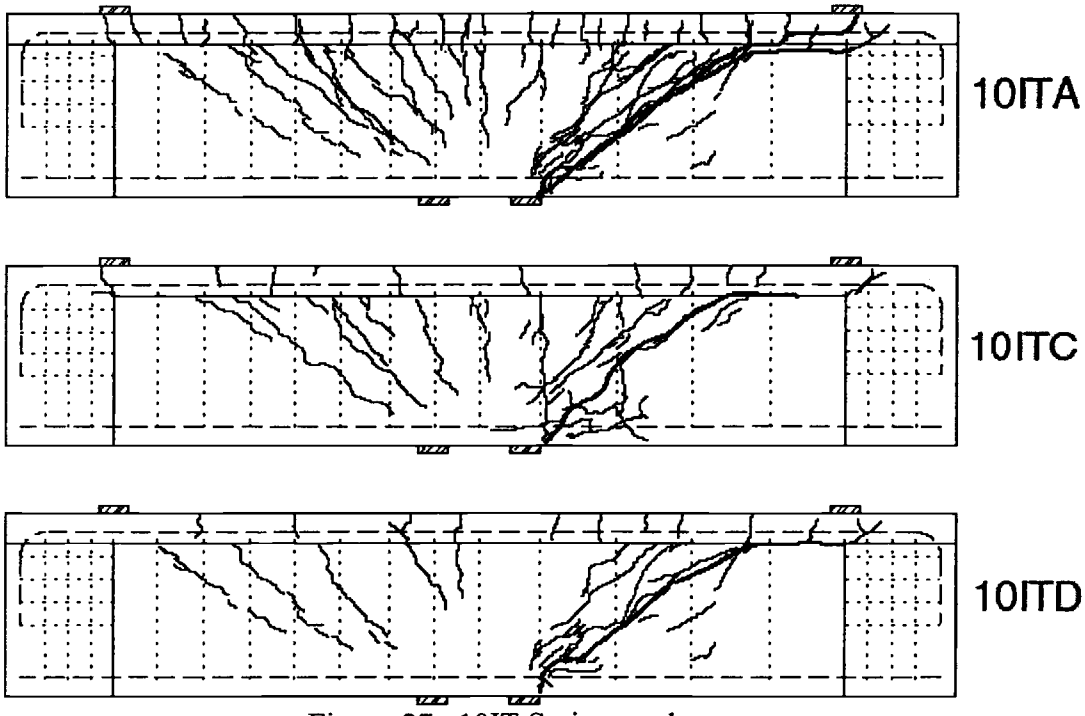

Figure 27: 10IT Series crack maps.

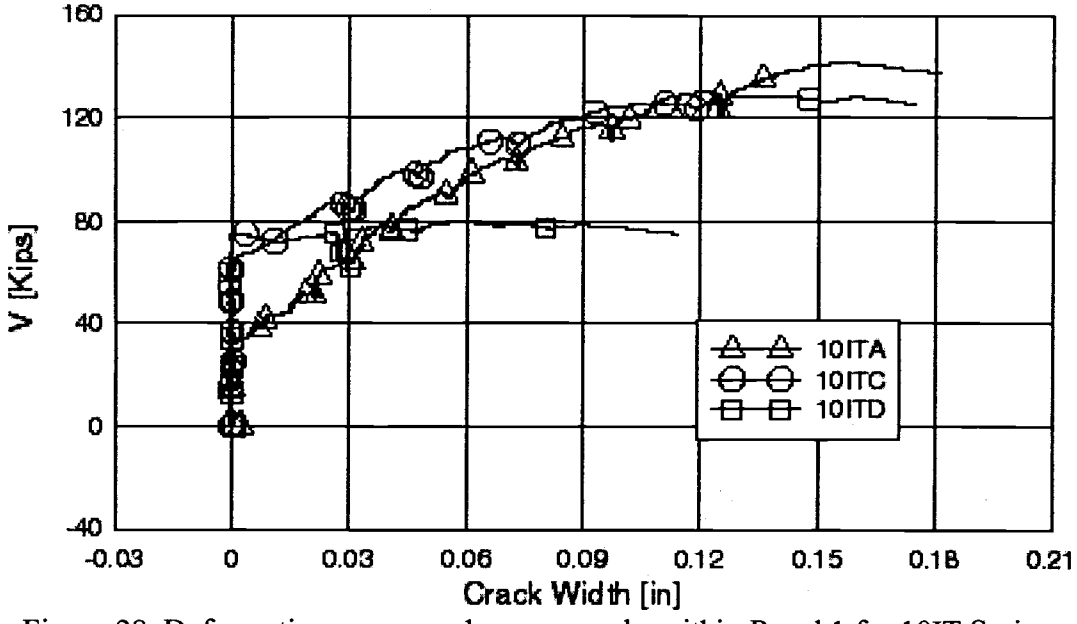

Figure 28: Deformations measured across cracks within Panel 1 for 10IT Series.

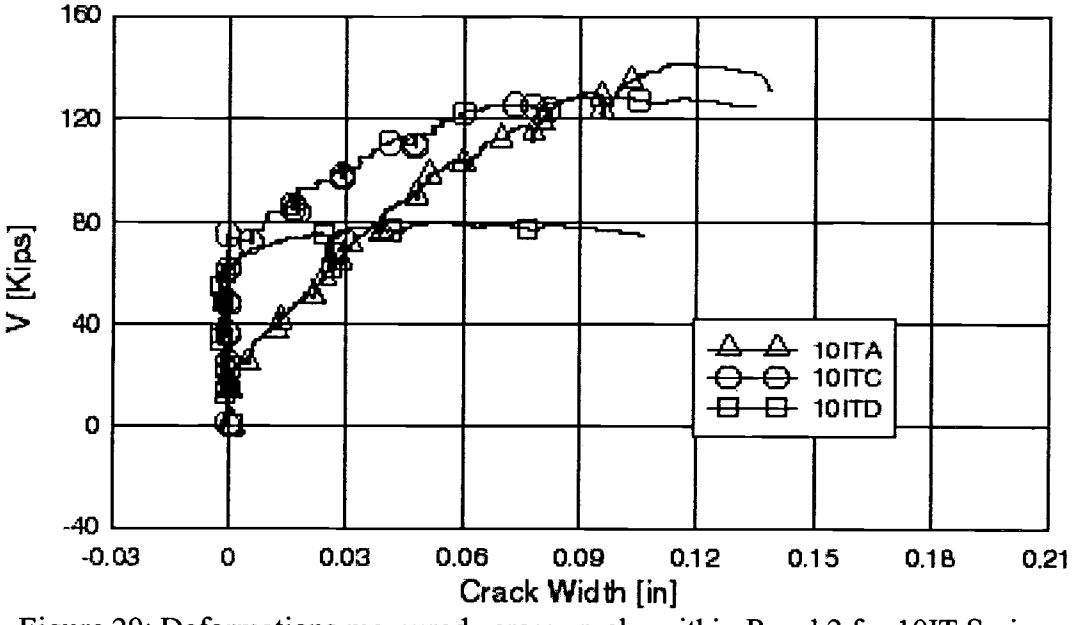

Figure 29: Deformations measured across cracks within Panel 2 for 10IT Series.

Beam Type	Corrosion Damage	f'_c [psi]	Stirrup Fracture	Load [kips]		Δ [in]	Percent Capacity
				P_{EXP}	V_{EXP}		
8R	A	4250	NO	267	133.5	0.47	100.0
	D		YES	212	106	0.39	79.4
10R	A	4850	NO	260	130	0.4	100.0
	B		NO	228	114	0.32	87.7
	C		YES	210	105	0.29	80.8
	D		YES	182	91	0.27	70.0
12R	A	4300	NO	220	110	0.47	100.0
	D		YES	199	99.5	0.35	90.5
10T	A	5300	NO	283	141.5	0.44	100.0
	C		YES	210	105	0.33	74.2
	D		YES	265	132.5	0.43	93.6
10IT	A	4650	NO	270	135	0.4	100.0
	C		NO	257	128.5	0.453	95.2
	D		YES	158	79	0.32	58.5

Table 9: Beam test summary tables.

Beam Type	Corrosion Damage	V_{EXP} [kips]	Δ [in]	V_{EXP} @ First Shear Crack	$50\%V_{EXP}$ [kips]	w_{cr} ($50\%V_{EXP}$) [in]	$75\%V_{EXP}$ [kips]	w_{cr} ($75\%V_{EXP}$) [in]
8R	A	133.5	0.47	37.5	62.5	0.016	100	0.025
	D	106.0	0.39	62.5		0.008		0.01
10R	A	130.0	0.4	50.0	62.5	0.013	100	0.02
	B	114.0	0.32	75.0		≤ 0.008		0.02
	C	105.0	0.29	62.5		≤ 0.008		0.025
	D_1	91.0	0.27	50.0		≤ 0.008		0.016
12R	A	110.0	0.47	37.5	50	≤ 0.008	75	0.02
	D	99.5	0.35	50.0		0.01		0.03
10T	A	141.5	0.44	50.0	75	.013 (+)	100	.016 (+)
	C	105.0	0.33	75.0		.016 (-)		0.04
	D	132.5	0.43	62.5		0.016		0.03
10IT	A	135.0	0.4	37.5	75	0.016	100	.02 (+)
	C	128.5	0.45	75.0		≤ 0.008		0.025
	D	79.0	0.32	50.0		≤ 0.008		0.06

Beam failed before 75-% V_{EXP}. Crack width taken at maximum at load step before failure

Table 10: Summary of crack widths.

5.3 Section Loss Measurement and Corrosion Products

Typical rebar damage states used in this study are shown in Figure 30. All corrosion damaged rebar exhibited significant areas of pitting. States B and C generally exhibited localized areas of section loss with only limited uniform loss along the length. Corrosion damage state D showed significant localized and uniform section loss and in many cases this damage state resulted in complete section loss at locations. On all stirrups the corrosion section loss was concentrated at the outside facing surface of the stirrup. For light and moderate corrosion specimens (B and C), the section loss tended to concentrate along the longitudinal rib. For moderate and severe damage states (C and D), both the longitudinal and transverse ribs on the rebar were significantly eroded. Typical examples of corrosion damage with areas of complete rebar section loss at crack locations identified after testing are shown in Figure 31. Fractures occurred at areas of significant section loss. Areas noted to have fractured at areas if localized section loss are shown in Figure 32. The most common locations for uniform section loss were at the top and bottom bend regions and can be seen in Figure 33.

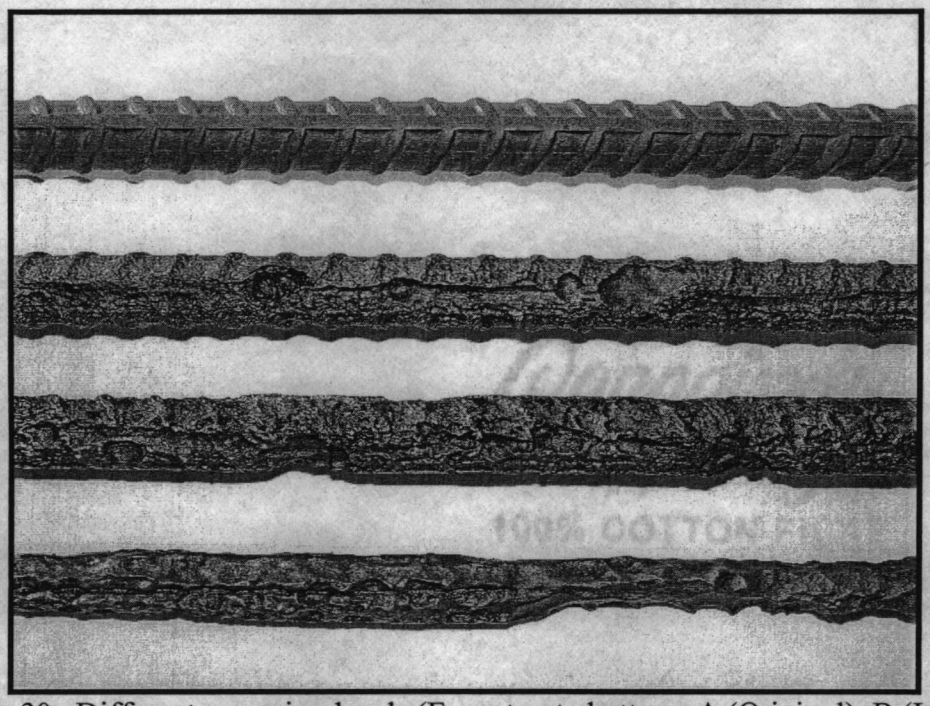

Figure 30: Different corrosion levels (From top to bottom, A (Original), B (Light), C (Moderate), D (Severe)).

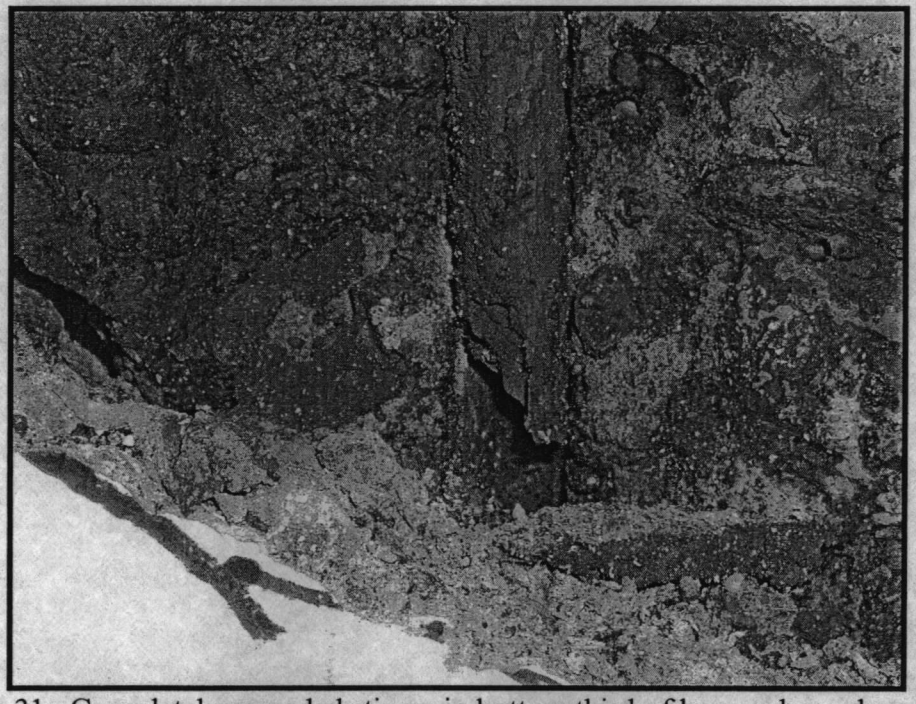

Figure 31: Completely corroded stirrup in bottom third of beam where shear crack formed.

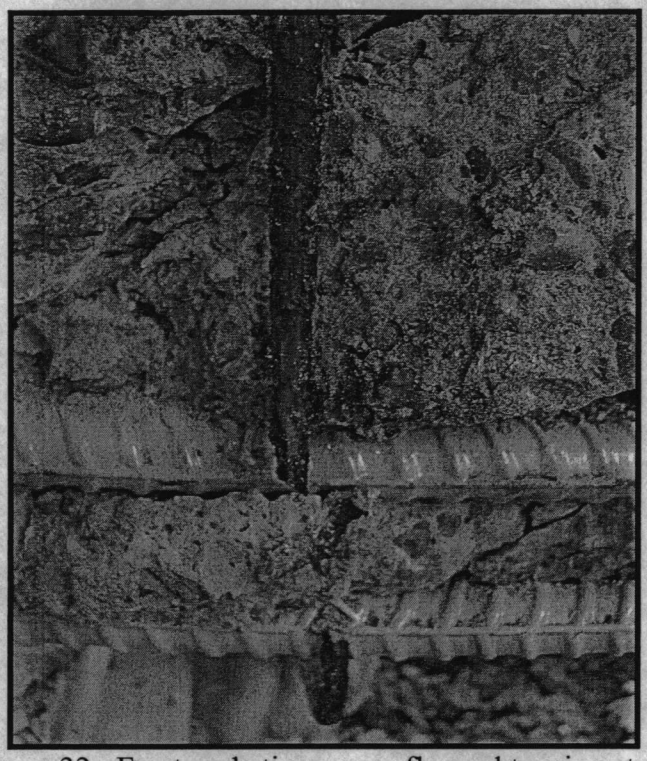

Figure 32: Fractured stirrup near flexural tension steel.

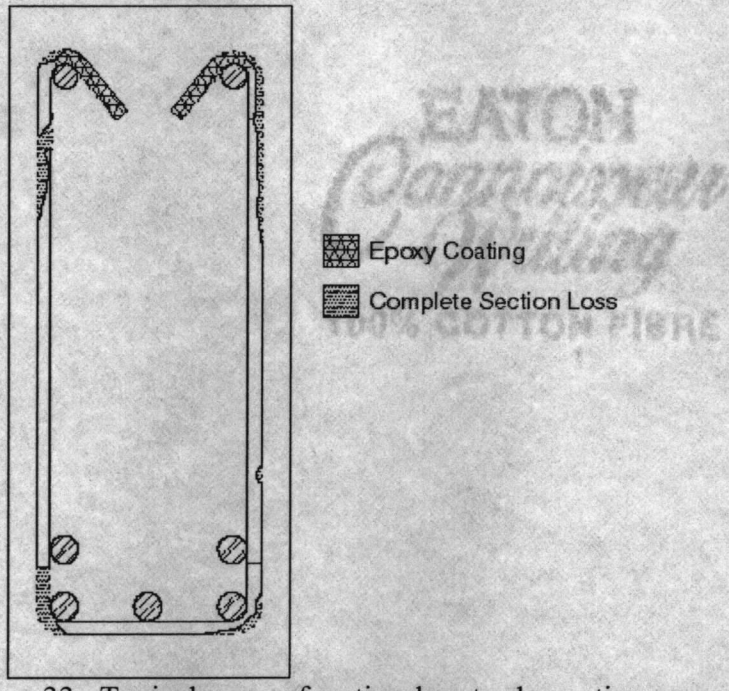

Figure 33: Typical areas of section loss to shear stirrup.

Immediately after strength testing, corrosion products were collected for examination using X-ray diffraction (XRD). Various iron oxide mineral species were found including magnetite (Fe_3O_4), akagenite (β-FeOOH), goethite (α-FeOOH), lepidocrocite (γ-FeOOH), and wuestite (FeO). The desired corrosion product, iron oxide $Fe(OH)_2$, has a higher volume ratio than most of the other iron oxide mineral species that were found except for the akagenite. This difference in volume expansion ratio may be another factor that contributed to the lack of the concrete cover spalling. The formation of magnetite and goethite is common in RC and occurs when the availability of oxygen varies, with magnetite forming when oxygen is limited and goethite when ample oxygen is available.

The corrosion section loss for each beam is reported three ways: (1) the average of all stirrups, (2) sum of maximum local section loss, and (3) maximum local section loss. Section loss measurements were for those stirrups that crossed the failure crack and are summarized in Table 12. The percent section loss was calculated based on the nominal area for a #4 bar (0.2 in^2). The amount of section loss can be quite different depending on the method chosen to quantify it. Even if a stirrup shows little section loss when measured using the average method, it could have a deep pit and/or a small area of extreme section loss that can lead to premature failure of the element. For example, specimen 10TC failed due to fracturing of two stirrups at locations of extreme section loss. The beam represented an intermediate damage state, and when quantifying the section loss based on the average value the section losses were 21% and 18% for stirrups S1

and S2, respectively. When determining the section loss based on local maximum the percent section losses were 62.5% and 73%, respectively.

Specimen	Average		Local Maximum		Local / Average	
	Area [in^2]	%Section Loss	Area [in^2]	%Section Loss	Area [in^2]	%Section Loss
8RD						
S2-1	0.147	26.7	0.110	45.0	0.75	1.69
S2-2	0.112	44.0	0.072	64.0	0.64	1.45
S3-1	0.151	24.3	0.145	27.5	0.96	1.13
S3-2	0.151	24.6	0.134	33.0	0.89	1.34
S4-1	0.153	23.5	0.106	47.0	0.69	2.00
S4-2	0.139	30.4	0.098	51.0	0.70	1.68
10RB						
S2-1	0.172	14.0	0.140	30.0	0.81	2.15
S2-2	0.175	12.7	0.156	22.0	0.89	1.73
S3-1	0.177	11.7	0.127	36.5	0.72	3.13
S3-2	0.171	14.6	0.128	36.0	0.75	2.47
10RC						
S2-1	0.158	20.9	0.155	22.5	0.98	1.08
S2-2	0.142	28.9	0.078	61.3	0.54	2.12
S3-1	0.161	19.7	0.144	28.0	0.90	1.42
S3-2	0.154	23.0	0.121	39.6	0.79	1.72
10RD						
S2-1	0.125	37.5	0.000	100.0	0.00	2.67
S2-2	0.112	43.9	0.046	77.0	0.41	1.76
S3-1	0.174	13.3	0.162	19.0	0.93	1.43
S3-2	0.183	8.5	0.158	21.0	0.86	2.47
12RD						
S1-1	0.144	27.8	0.102	49.0	0.71	1.76
S1-2	0.133	33.3	0.133	33.5	1.00	1.01
S2-1	0.115	42.3	0.000	100.0	0.00	2.36
S2-2	0.137	31.6	0.010	95.0	0.07	3.01
10TC						
S1-1	0.143	28.7	0.089	55.5	0.62	1.93
S1-2	0.172	14.2	0.075	62.5	0.44	4.40
S2-1	0.191	4.3	0.054	73.0	0.28	16.98
S2-2	0.137	31.4	0.148	26.0	1.08	0.83
10TD						
S2-1	0.145	27.3	0.105	47.5	0.72	1.74
S2-2	0.114	43.2	0.000	100.0	0.00	2.31
S3-1	0.167	16.4	0.149	25.5	0.89	1.56
S3-2	0.113	43.6	0.000	100.0	0.00	2.29
10TTC						
S2-1	0.159	20.3	0.142	29.0	0.89	1.43
S2-2	0.167	16.4	0.145	27.5	0.87	1.68
S3-1	0.165	17.8	0.148	26.0	0.90	1.46
S3-2	0.170	15.2	0.149	25.5	0.88	1.68
10TTD						
S2-1	0.090	54.9	0.056	72.0	0.62	1.31
S2-2	0.149	25.5	0.113	43.5	0.76	1.71
S3-1	0.153	23.4	0.123	38.5	0.80	1.65
S3-2	0.121	39.6	0.067	66.5	0.55	1.68

Table 11: Average and local maximum section losses for stirrups crossing the failure crack.

Beam Type	Corrosion Damage	Measured Area [in^2]			Percent Section Loss		
		1	2	3	1	2	3
8R	A	0.20	0.60	0.20	0.0	0.0	0.0
	D	0.142	0.304	0.072	28.9	49.3	64.0
10R	A	0.20	0.40	0.20	0.0	0.0	0.0
	B	0.174	0.267	0.127	13.2	33.3	36.5
	C	0.154	0.198	0.079	23.1	50.4	60.5
	D	0.148	0.158	0.0	26.0	60.5	100.0
12R	A	0.20	0.40	0.20	0.0	0.0	0.0
	D	0.133	0.102	0.0	33.8	74.5	100.0
10T	A	0.20	0.40	0.20	0.0	0.0	0.0
	C	0.161	0.129	0.054	19.7	67.8	73.0
	D	0.135	0.00	0.0	32.6	100.0	100.0
10IT	A	0.20	0.40	0.20	0.0	0.0	0.0
	C	0.165	0.290	0.142	17.4	27.5	29.0
	D	0.128	0.123	0.056	35.9	69.3	72.0

Table 12: Percent Section Loss due to Corrosion (Section Loss: 1=Average of all stirrups in test span, 2=Sum of Local Maximum for all stirrups in test span, 3= Local Maximum Section Loss).

5.4 Capacity Loss Determination

The amount of capacity loss was compared to the amount of stirrup section loss using the three methods described previously. The 10R Series capacity loss is shown in Figure 34 and compared against the 16th Edition of the AASHTO Standard Specification (AASHTO, 1996) equations for shear resistance:

$$V_n = V_c + V_s \qquad [8]$$

$$V_c = 2\sqrt{f'_c}\, b_w d \qquad [9]$$

$$V_s = \frac{A_v f_y d}{s} \qquad [10]$$

Using average section loss to characterize the beam gives a degradation curve that appears quite severe. It is unlikely that the subtle change in area from 24% to 26% would cause such a dramatic drop in shear capacity. The second method uses

the sum of the local maximum section losses for the two critical stirrups. Here also, the response appears to be nonlinear with large decreases in shear capacity with small increases in section loss. By using the maximum section loss within the critical section (Method 3) the shear capacity drop off becomes linearly related to the local maximum section loss. The slope of this line fits well with the ACI approach assuming that only the area of the stirrups decreases.

The effect of stirrup spacing and cross-sectional shape on shear capacity loss is compared using the three section loss calculation methods: average, sum of local maximums, and local maximums. The capacity loss was normalized for all beam series. The percent capacity was determined by dividing the maximum shear force for the corroded specimen by the maximum shear force from the corresponding uncorroded specimen (A), as shown in Table 13. The percent capacity using Method 1 is shown in Figure 35. This method gives significant capacity reduction at small values of percent section loss. However, the average section loss measurement was not representative of the damage that occurred to the stirrups, particularly due to debonding. Method 2 showed a reasonable trend for the capacity loss as shown in Figure 36. Method 2 better represents the critical stirrup damage that occurred. Method 3 results are shown in Figure 37 and trends are similar to Method 2. Two of the beams, 10RD and 12RD, were significantly different due to the fact that both beams had one stirrup that had undergone more section loss than the other stirrup that was deemed critical. The percent change in deflection versus Method 3 is shown in Figure 38.

Beam Type	Corrosion Damage	V [kips]	Δ [in]	Percent Section Loss			$\frac{V_{MAX}}{V_{MAX}(\text{no corrosion})}$
				1	2	3	
8R	A	133.5	0.47	0.0	0.0	0.0	100.0
	D	106.0	0.39	28.9	49.3	64.0	79.4
10R	A	130.0	0.40	0.0	0.0	0.0	100.0
	B	114.0	0.32	13.2	33.3	36.5	87.7
	C	105.0	0.29	23.1	50.4	60.5	80.8
	D	91.0	0.27	26.0	60.5	100.0	70.0
12R	A	110.0	0.47	0.0	0.0	0.0	100.0
	D	99.5	0.35	33.8	74.5	100.0	90.5
10T	A	141.5	0.44	0.0	0.0	0.0	100.0
	C	105.0	0.33	19.7	67.8	73.0	74.2
	D	132.5	0.43	32.6	100.0	100.0	93.6
10IT	A	135.0	0.40	0.0	0.0	0.0	100.0
	C	128.5	0.45	17.4	27.5	29.0	95.2
	D	79.0	0.32	35.9	69.3	72.0	58.5

Table 13: Percent capacity due to corrosion damage compared against three section loss methods (1=Average of all stirrups in test span, 2=Sum of Local Maximum of all stirrups in test span, 3=Local Maximum Section Loss).

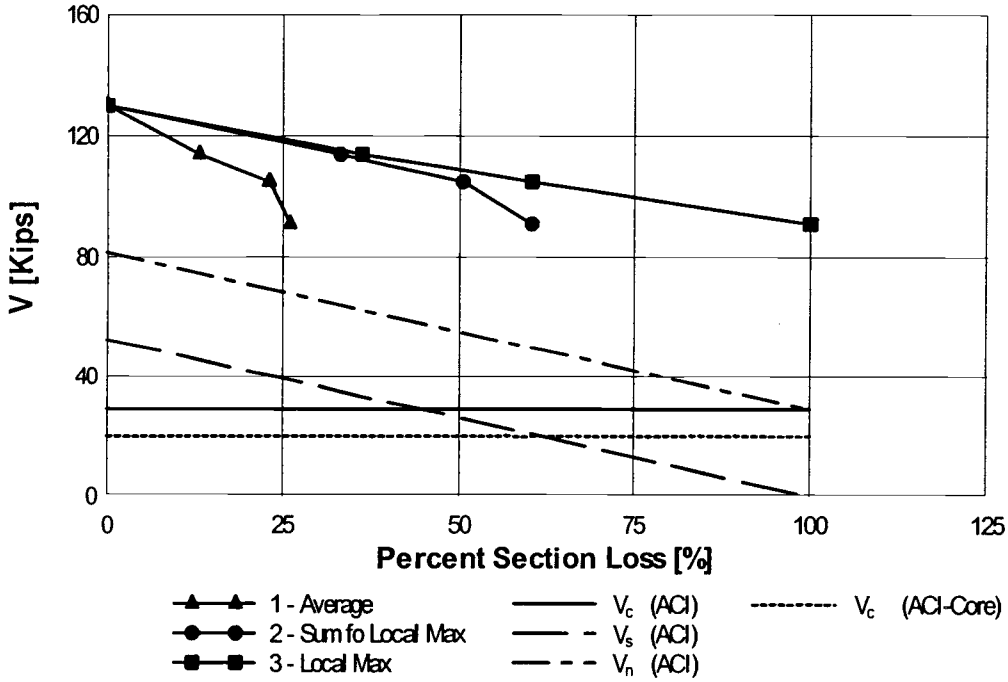

Figure 34: Shear capacity versus section loss plot for 10R Series.

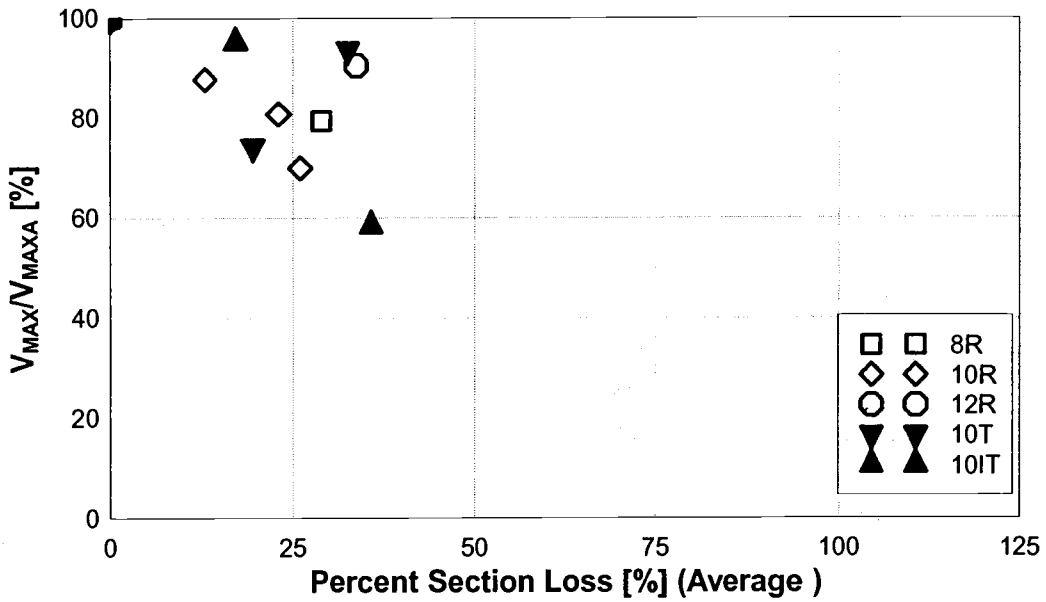

Figure 35: Percent shear capacity versus average percent section loss plot.

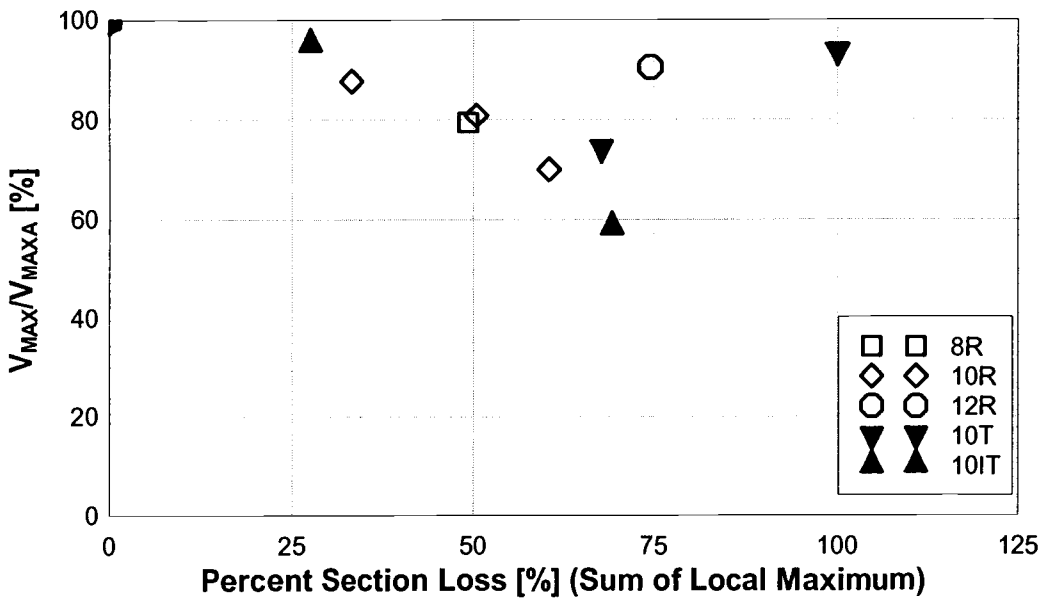

Figure 36: Percent shear capacity versus sum of local maximum section loss

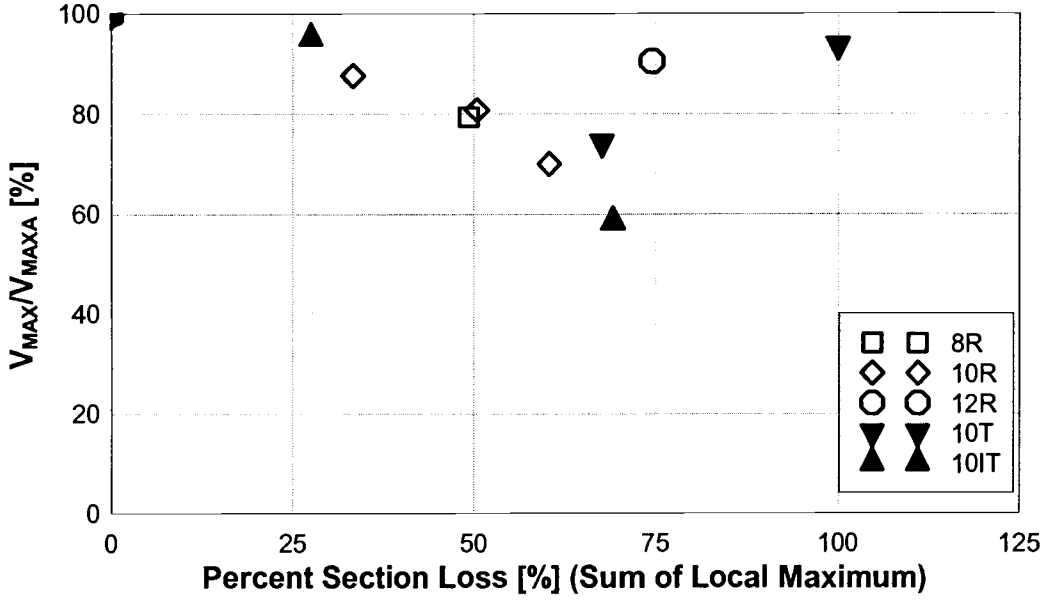

Figure 37: Percent shear capacity versus Local Maximum Section Loss

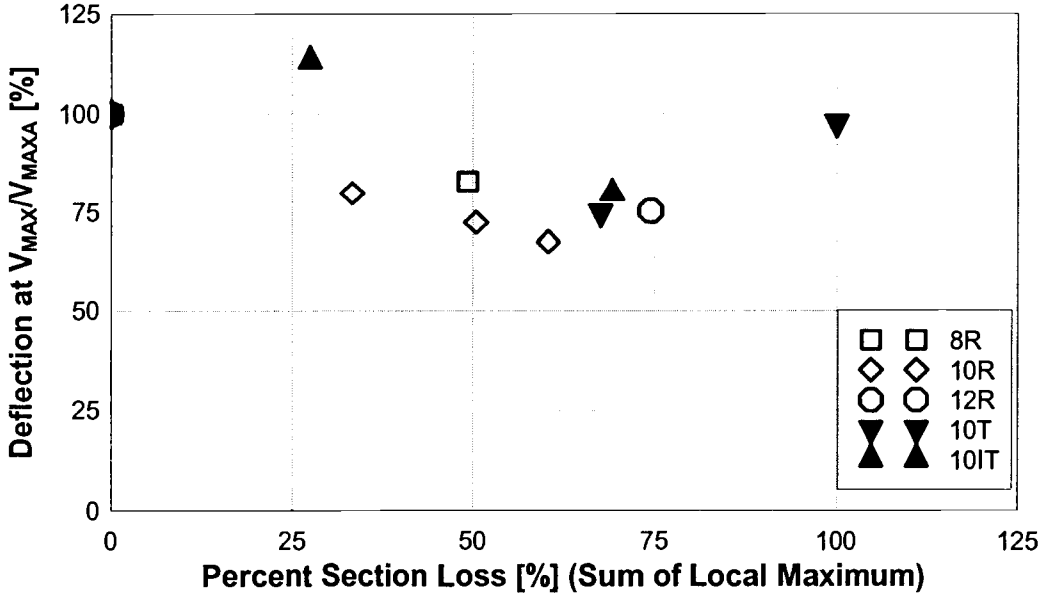

Figure 38: Deflection at V_{MAX} versus the Sum of the Local Maximum section losses.

6.0 Conclusions

A research program on the structural performance of CRC beams that had undergone corrosion damage to the embedded shear reinforcing steel was performed. Visual signs of corrosion distress were correlated with structural performance of CRC beams that were corroded to four damage states. Rebar section loss was quantified using three methods. The following conclusions are made:

- Section loss of the reinforcing steel due to corrosion was not uniform along the length of the stirrup. Significant local pitting damage was observed, particularly at higher damage states.
- Stirrup spacing changed the extent of damage to the concrete due to expansion of corrosion products. In areas of tightly spaced stirrups the cover cracking overlaps and causes greater areas of delaminations and/or spalling. When stirrups are widely spaced, the damage to the concrete is more localized.
- The locally reduced section can lead to localized yielding and reduced ductility.
- Fracture can occur at severely corroded locations on stirrups.
- The location and severity of corrosion damage to the reinforcing steel can reduce ductility and capacity of the section in shear.

- Corrosion damage occurring to the concrete is dependent on the type and quantity of the corrosion products.
- Corrosion damage reduces the ability of the stirrup to confine the width of the shear crack(s) that crosses that stirrup.
- Shear cracking did not occur at lower loads for the corroded specimens. This indicates that cover does not appear to be as significant as the concrete core contribution to shear strength.
- Remaining capacity of corroded beams was best described using the maximum local section loss of stirrups within the critical shear crack region.
- Current inspection techniques may not accurately indicate the structural performance of CRC beams that have undergone corrosion.
- Inspections should identify stirrups within a span length equal to the beam depth to identify sequential reduced stirrup sections
- It is likely that bridge girders with significant rebar corrosion and localized section loss may fail abruptly after shear cracking of the concrete core.

Bibliography

AASHTO T 260-94, "Sampling and Testing for Chloride Ion in Concrete and Concrete Raw Materials," Standard Specifications for Transportation Materials and Methods of Sampling and Testing, 17th Edition, Part II, 1995.

ACI 318, "Building Code Requirements for Structural Concrete," American Concrete Institute, Farmington Hills, Michigan, 1999.

Almusallam, A. A., Al-Gahtani, A. S., Aziz, A. R., Dakhil, F. H., Rasheeduzzafar, "Effect of Reinforcement Corrosion on Flexural Behavior of Concrete Slabs," *Journal of Materials in Civil Engineering*, ASCE, V. 8, No. 3, 1996, pp 123-127.

Almusallam, A. A., "Effect of Degree of Corrosion on the Properties of Reinforcing Steel Bars," *Construction and Building Materials*, Elsevier Science Limited, V. 15, 2001, pp 361-368.

Al-Sulaimani, G. J., Kaleemullah, M., Basunbui, I. A., Rasheeduzzafar, "Influence of Corrosion and Cracking on Bond Behavior and Strength of Reinforced Concrete Members," *ACI Structural Journal*, ACI, V. 87, No. 2, 1990, pp 220-231.

Amleh, L., Mirza, S. "Corrosion Influence on Bond between Steel and Concrete," *ACI Structural Journal*, ACI, V. 96, No. 3, 1999, pp 415-423.

ASCE-ACI Committee 445 "Recent Approaches to Shear Design of Structural Concrete," *Journal of Structural Engineering*, V. 124, No. 12, 1999, pp 1375-1417.

ASTM G 1-99, 2001, "Standard Practice for Preparing, Cleaning, and Evaluating Corrosion Test Specimens," *1996 Book of ASTM Standards, Section 1: Iron and Steel Products*, V. 3.02, pp 9-21.

Bentur, A., Diamond, S., Berke, N. S., "Steel Corrosion in Concrete," E & FN Spon, New York, NY, 1997.

Cabrera, J. G. "Deterioration of Concrete Due to Reinforcement Steel Corrosion," *Cement & Concrete Composites*, Elsevier Science Limited, V. 18, 1996, pp 47-59.

Covino, B. S., Cramer, S. D., Holcomb, G. R., Bullard, S. J., Laylor, H. M. "Postmortem of a Failed Bridge," *Concrete International*, ACI, 1999, pp 39-45.

Cramer, S. D., Covinp, B. S., Bullard, S. J., Holcomb, G. R., Russell, J. H., Nelson, F. J., Laylor, H. M., Soltesz, S. M., "Corrosion Prevention and Remediation Strategies for Reinforced Concrete Coastal Bridges," *Cement and Concrete Composites*, V. 24, 2002, pp 101-117.

"FHWA-RD-01-156: Corrosion Cost and Preventive Strategies in the United States," FHWA, McClean, VA, March 2002.

Francois, R., Arliguie, G., "Influence of Service Cracking on Reinforcement Steel Corrosion," *Journal of Materials in Civil Engineering*, ASCE, V. 10, No. 1, February 1998, pp 14-20.

Kay, T., "Assessment and Renovation of Concrete Structures", Longman Scientific & Technical, New York, NY, 1992.

"LRFD Bridge Design Specifications, Second Edition", AASHTO, Washington, D. C., 2002.

"Oregon Department of Transportation Bridge Inspection Pocket Coding Guide," Oregon Department of Transportation, Salem, OR, 2001.

Palsson, R., Mirza, M. S., "Mechanical Response of Corroded Steel Reinforcement of Abandoned Concrete Bridge," *ACI Structural Journal*, ACI, V. 99, No. 2, 2002, pp 157-162.

"Standard Specification for Highway Bridges, Sixth Edition", AASHTO, Washington, D. C., 1953.

"Standard Specification for Highway Bridges, Sixteenth Edition", AASHTO, Washington, D. C., 1996.

Stanish, K, Hooton, R. D., Pantazopoulou, S. J., "Corrosion Effects on Bond Strength in Reinforced Concrete," *ACI Structural Journal*, ACI, V. 96, No. 6, 1999, pp 915-921.

Appendix

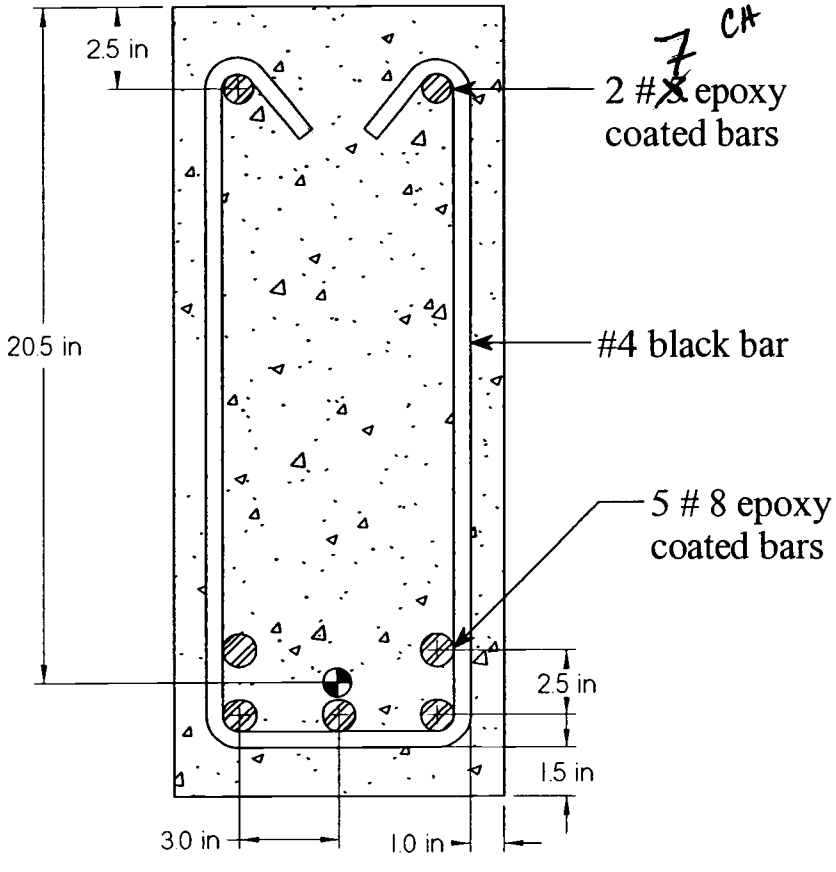

TYPE I cross-section

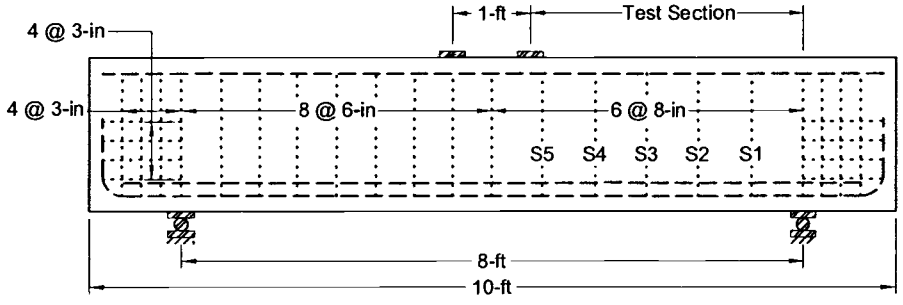

8R Series

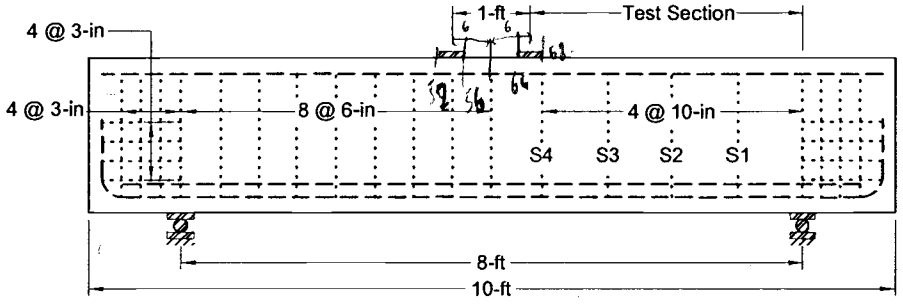

10R Series

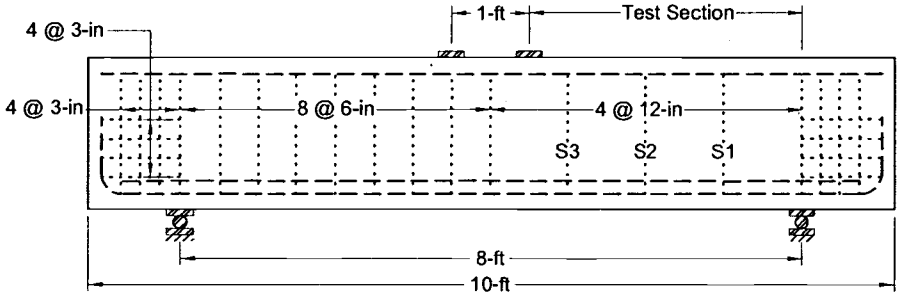

12R Series

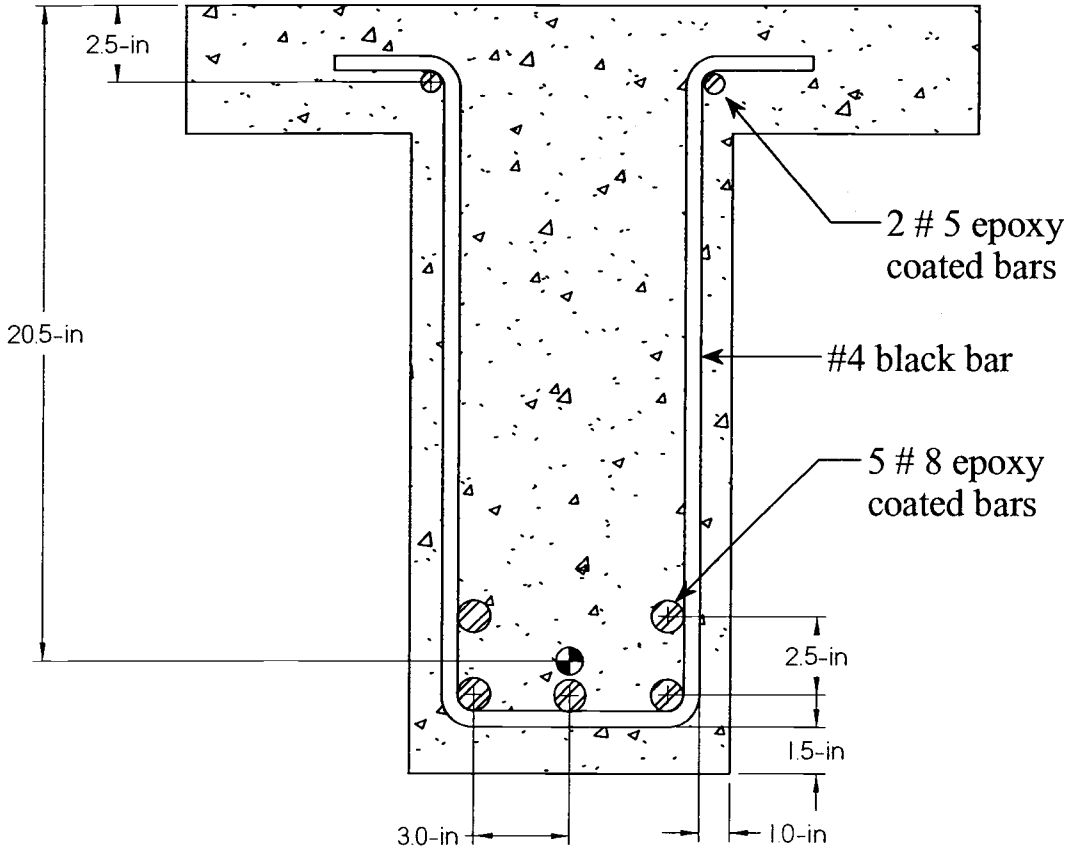

TYPE II cross-section

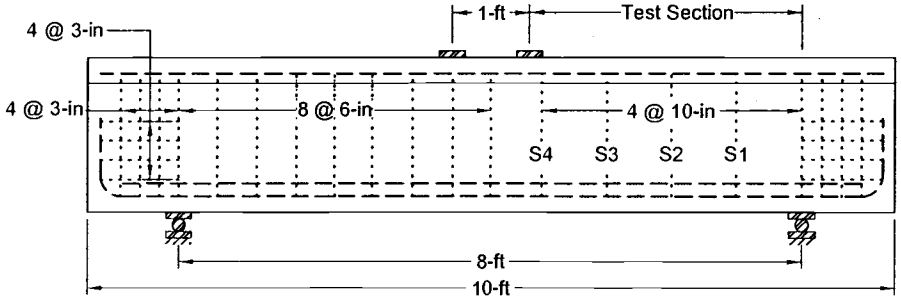

Side View

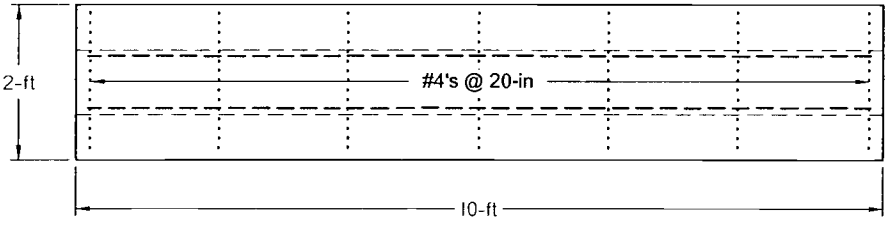

Top View

10T Series

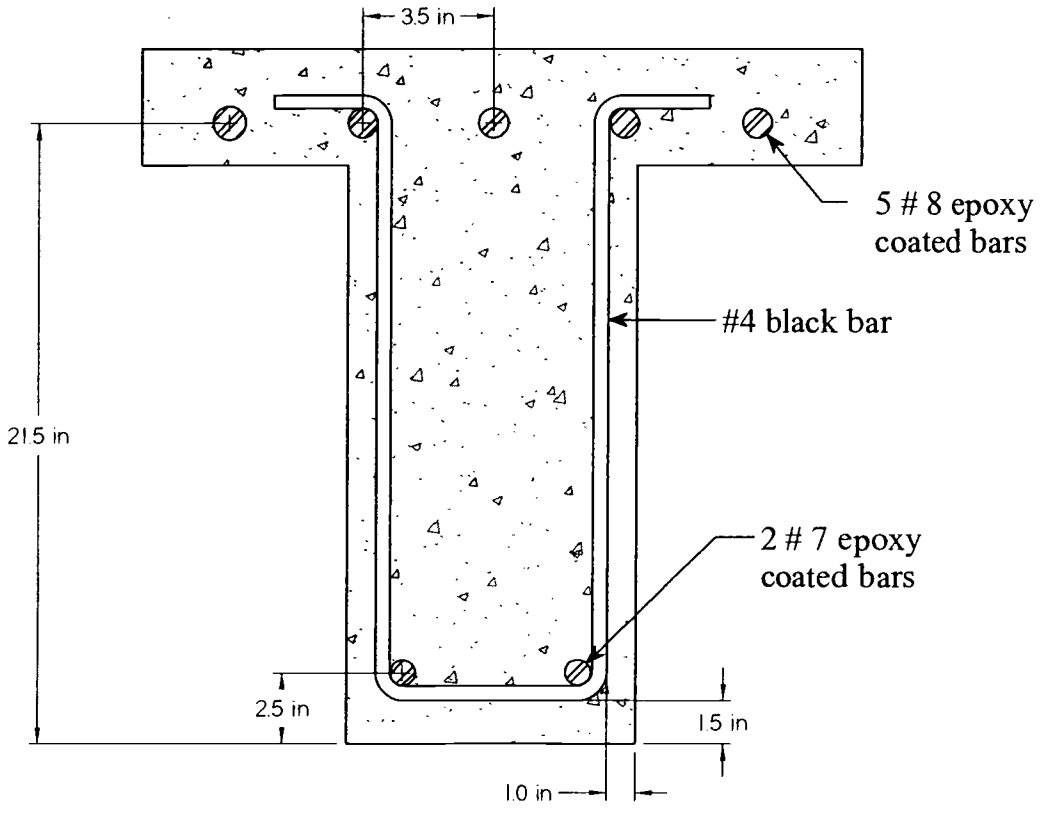

TYPE III Cross-section

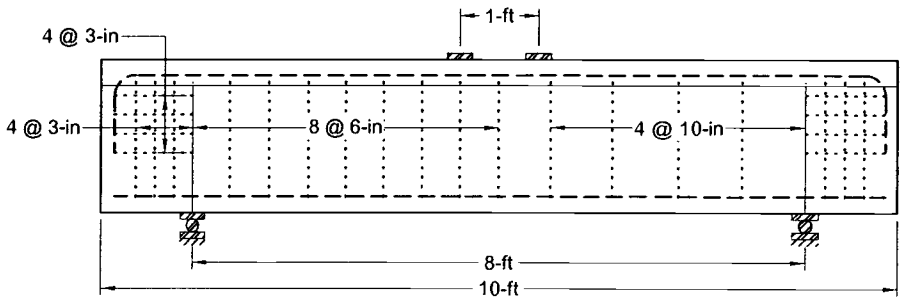

Side View

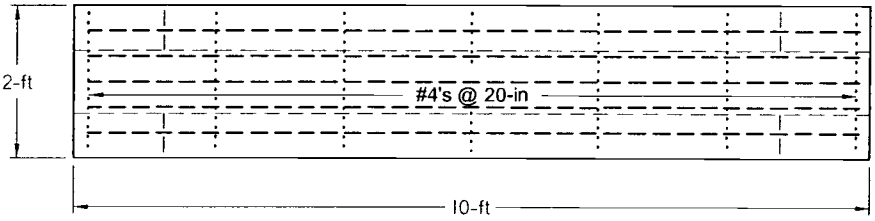

Top View

10IT Series